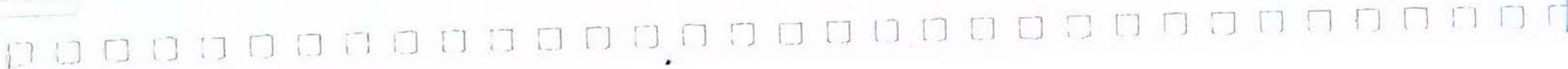


ENG 220-(EQC 1993/103)

Precast Concrete Floor Unit Support and Continuity Report on the performance of current details: effects of frame dilation and translation on extruded hollow core flooring

M D Herlihy, Department of Civil Engineering, University of Canterbury (Supervised by: Professor R Park, Mr D K Bull)



ENR
220

Project 93/103 Precast Concrete Floor Unit Support and Continuity

Report on the performance of current details: effects of frame dilation and translation on extruded hollow core flooring

This report submitted to the Earthquake Commission documents the results and recommendations from laboratory tests conducted at the Department of Civil Engineering of the University of Canterbury during 1994

by

M D Herlihy
ME Student

Supervised by: Professor R Park
Mr D K Bull

May 1995

Abstract

Three tests were undertaken to investigate the adequacy of typical precast Hollow Core flooring support details used by structural designers throughout New Zealand. The emphasis of these tests was to determine the ability of standard details to withstand displacement type loadings associated with the differential movements of support members during a severe earthquake. The testing regimes were so arranged to examine two separate types of frame-to-frame or frame-to-wall support displacement formats, as follows:

The first two tests involved direct loss of support, as caused by the axial dilation of plastic hinges in seismic load resisting frame members, or any similar movements caused by volumetric changes which may result in a loss of support integrity. These tests examined the common support detail with its full reliance on composite topping bond, as well as a special reinforcing detail recommended by Firth Stresscrete for short seatings. These tests followed a format earlier employed at the University of Canterbury to verify the performance of recommended reinforcing details for maintaining structural integrity at supports. Provision was made for an applied vertical load to test the shear performance of these details.

The third experiment involved a new test assembly which specifically examined the ability of Hollow Core units to sustain excessive compression stresses in the exterior web and soffit regions under translational displacements. This assembly also demanded that a degree of bond performance must occur between the precast unit and composite topping to sustain the lateral load, and thus examined the ability of the topping slab to transfer diaphragm shear as assumed in design. A vertical load was applied at mid span prior to the main test to cause cracking along the support lines, thus simulating the formation of cracks caused by service loads and volume changes in a real structure. Measurements of starter and continuity bar stresses were taken at all these stages of loading to assess the expected levels of "top steel" stress in the floors of real structures under service loads. The applied axial compression load used in this test was based on the geometry of a Los Angeles building that exhibited failure of Hollow Core units in the January 1994 earthquake, and was calculated from the seismic loading provisions of the New Zealand loadings code.

Contents

Abstract	ii
Contents	iii
Notation	vi
Chapter 1: Introduction	
1.1 General	1
1.2 Previous Research	2
1.3 Objectives of Research	3
Chapter 2: Loss of Support through Axial Displacement	
2.1 General	5
2.2 Description of Test Rig	
2.2.1 Horizontal Displacement	7
2.2.2 Vertical Force	8
2.3 Instrumentation	
2.3.1 Hydraulic Ram Forces	9
2.3.2 External Displacements	9
2.3.3 Bar Strains	10
2.3.4 The Data Logger Unit	10
Chapter 3: Loss of Support: Test A	
3.1 Description of Support Detail	11
3.2 The Detail Tested	13
3.3 Materials	13
3.3.1 Concrete	13
3.3.2 Reinforcing Steel	14
3.4 Results of Test	15
3.5 Analysis of Test Results	15
(I) Peak Load and Fracture	17
(II) Post-Fracture to Post Fracture Peak Load	21
(III) Post-Fracture Peak Load to Full Loss of Reaction	24
(IV) Loss of Reaction to Failure	25
3.6 General Analysis	27
3.6.1 Fracture of the Hollow Core at the Support	27
3.6.2 Work Done	30

3.6.3 Composite Topping Bond	30
3.7 Conclusions from Test A	33
3.8 Recommendations from Test A	33
3.9 Recommendations for Future Research	35
Chapter 4: Loss of Support: Test B	
4.1 Description of Support Detail	36
4.2 The Detail Tested	37
4.3 Materials	
4.3.1 Concrete	38
4.3.2 Reinforcing Steel	38
4.4 Results of Test	39
4.5 Analysis of Test Results	39
(I) Loss of Concrete Tension	41
(II) Post-Cracking to Peak Load	42
(III) Peak Load to Loss of Mesh	43
(IV) Plateau Region to onset of Hairpin Fracture	45
(V) Hairpin Fracture to End of Test	45
4.6 General Analysis	
4.6.1 Ductility and Work Done	45
4.6.2 Dowel Action at the Support	46
4.7 Conclusions from Test B	47
4.8 Recommendations from Test B	47
4.9 Recommendations for Future Research	48
Chapter 5: Translation and Diaphragm Action	
5.1 General	49
5.2 Description of Test Rig	51
5.2.1 Translation and Axial Load	53
5.2.2 Vertical Loads	53
5.3 Instrumentation	53
5.3.1 Hydraulic Ram Forces	53
5.3.2 External Displacements	53
5.3.3 Bar Strains	54
5.3.4 The Data Logger Unit	54
Chapter 6: Sway and Axial Load: Test A	
6.1 Description of Support Detail	55

6.2 The Detail Tested	55
6.3 Materials	
6.3.1 Concrete	55
6.3.2 Reinforcing Steel	56
6.4 Axial Load and Test Format	56
6.5 Results of Initial Loading	57
6.6 Analysis of Results from Initial Loading	58
6.7 Results from Second Loading	62
6.8 Analysis of Results from Second Loading	64
6.9 Conclusions of the Sway and Axial Load Test	64
6.10 Recommendations from Sway and Axial Load Test	65
6.11 Recommendations for Future Research	66
References	67

Notation

A_b	= area of a reinforcing bar
A_s	= area of reinforcing steel
A_{sm}	= area of mesh wire
A_{pc}	= area of precast section
A_{vf}	= area of reinforcing steel for developing shear friction
A'_g	= transformed area of the total section
b	= width of section or of building, as appropriate
C	= lateral force coefficient
c	= depth to neutral axis from extreme compression fibre
C_c	= compression force in concrete
C_h	= basic seismic acceleration coefficient
d	= effective depth of section
d_b	= diameter of reinforcing bar
E_c	= elastic modulus of concrete
E_s	= elastic modulus of reinforcing bars
E_{sm}	= elastic modulus of mesh wire
f_{cx}	= stress in concrete acting in direction x (axial)
f_s	= stress in reinforcing steel
f_{si}	= stress in bar number i in a layer
f_{sm}	= stress in mesh wire
f_{su}	= ultimate stress capacity of reinforcing steel
f_y	= nominal yield stress of reinforcing steel
f'_c	= crushing strength of concrete test cylinder
f_t	= principal tensile stress
G	= gravity load
l_d	= development length of reinforcing bar
L_o	= gauge length
L_u	= limit state factor for the ultimate limit state
M	= bending moment
P_{δ_i}	= horizontal force corresponding to displacement i
P_{pc}	= force in precast section
P_{max}	= maximum force in section
P_u	= factored axial load occurring simultaneously with shear at a section
Q	= reduced live load
R	= risk factor for a structure

- s = spacing of reinforcing bars in a layer
 S_p = structural performance factor
 u = bar bond stress
 $U_{\delta p}$ = strain energy due to inelastic displacement
 U_{ext} = external work done
 U_{int} = internal strain energy
 V_d = shear force carried by bar kinking
 v_h = allowable horizontal shear stress in composite construction
 W = weight (load)
- α = deviation angle of bar
 β_1 = ratio of equivalent concrete stress block depth to the neutral axis depth
 δ = displacement
 δ_i = displacement i in a series
 Δ_c = change in section depth
 Δ_ϵ = change in strain
 Δ_y = displacement at yield
 Δ_u = displacement at a limit state
 ϵ_c = strain in concrete at extreme fibre
 ϵ_{si} = strain in reinforcing bar i
 ϵ_u = ultimate strain capacity of reinforcing
 ϕ = capacity reduction factor
 μ = coefficient of friction
 v = shear stress
 θ_p = orientation of principal tensile stress plane in relation to axial stress plane
 ψ = curvature
 ψ_u = live load combination factor

Chapter 1. Introduction

1.1 General

Section eight of the current New Zealand code of practice NZS 3101: 1982 " The Design of Concrete Structures" [1] contains some relatively straight forward requirements for the development of horizontal shear bond between precast concrete elements and composite concrete topping. In circumstances where precast elements are produced by placing concrete at slumps typically greater than 60mm, the surface roughening amplitude and tie reinforcement requirements specified in this code are readily obtained. On the other hand, with extruded systems where zero slump concrete is necessary, it is not possible to embed tie reinforcement economically, and it is difficult to roughen the extruded surface to any significant degree of amplitude. The premise that composite bond can be developed between the extruded element and topping alone is primarily based on tests conducted by the manufacturers of extrusion plant, and is hence reported to the purchasers of these proprietary systems (ie. the precaster) as part of the sale agreement.

Concerns about splitting of the webs and soffit of Hollow Core slabs have come about only as recently as the Los Angeles earthquake of January 1994. In this event, an unprecedented floor failure occurred in which longitudinal web splitting and topping delamination, due to combinations of diaphragm "beam" action and differential support movements, contributed to part of an observed structural failure (Fig. 1.1):



**Fig 1.1: Hollow Core floor failure exhibiting fracture of web elements
(Los Angeles 1994)**

1.2 Previous Research

Results of tests by extrusion plant manufacturers do not appear in common sources of literature, however, some tests that have examined composite topping bond to extruded flooring surfaces are evident. An important reference is that of Scott [2] in which an "as extruded" Hollow Core unit of 9.6m clear span was shown to develop full composite bond at flexural capacity under a superimposed load of 6.5 kPa. In section 2.6 of "The Guidelines for the Use of Structural Precast Concrete in Buildings" [3], reference is made to the composite bond characteristics of extruded flooring units, and the important issue of surface roughening amplitude.

Other references, in particular those from the European authority, FIP [4,5] conclude that a sufficient level of composite bond is available on extruded surfaces to sustain horizontal shear under normal levels of gravity loading. The European approach to horizontal shear stress at the topping interface is to consider Hollow Core flooring as a "low shear" application. Table 1 [5] shows a comparison of the ultimate limit state horizontal shear stresses for composite slabs, with extruded flooring top surfaces being considered as "naturally rough".

Grade of in situ concrete		f_{cu}	25	30	40 and over
			N/mm ²	N/mm ²	N/mm ²
Maximum shear stress	Intentionally rough	$0.025f_{cu}$	0.625	0.750	0.800
	Naturally rough	$0.015f_{cu}$	0.375	0.450	0.500
	Smooth	Values to be determined by test – See Appendix B			

Table 1.

Because this data is based on the 28 day crushing strengths of cubes and not cylinders, an approximate correction factor of 1.25 should be applied, thus, the allowable ultimate shear stress becomes:

$$v_h = 0.019 f'_c$$

From this equation, and a more complex related equation [4], it is evident that for topping concretes of relatively low compressive strength, a lower value of allowable horizontal shear may need to be considered than the 0.55 MPa specified in the current New

Zealand design code. The FIP publications are also quite particular about the influence of site construction practices and topping concrete mix design on the eventual effective bond between the precast unit and the topping. An important consideration reported in these documents [4,5] is the need to assess accidental loads, dynamic or seismic loads and the effects of differential shrinkage separately from the general "low shear" limit state format that does not require reinforcing at the composite interface.

*No apparent literature exists on composite bond performance under loads that directly result from structural interaction in the support region.

With regard to design details for overcoming loss of support problems, the experiments conducted by Mejia and Park [6] clearly indicate that satisfactory details can be employed to maintain structural integrity in situations of support loss, or where short seatings occur (Fig. 1.2). The principles of these details are in keeping with those that appear in two useful publications of precast concrete practice guidelines [3,7].

Obviously, no relevant information exists to date regarding the web splitting characteristics of Hollow Core flooring under translational loadings.

1.3 Objectives of Research

The principal aim of this initial phase of research was to:

- Establish the performance of composite bond in the role of restraining extruded Hollow Core flooring members onto the supports and the effectiveness of shear transfer through the topping slab, via starter and continuity bars.
- Determine the horizontal force-displacement characteristics and vertical shear capacity of a standard detail recommended by Firth Stresscrete for short seating applications.
- Determine whether the translational displacement of supports is a significant component that may cause web splitting in Hollow Core flooring elements under similar diaphragm load conditions that occurred in the Los Angeles earthquake of January 1994.
- Establish the typical levels of starter and continuity bar stresses under typical floor service loads.

- Utilise the information gained from these tests to both enhance existing details and develop specific details to mitigate any problems that might appear.

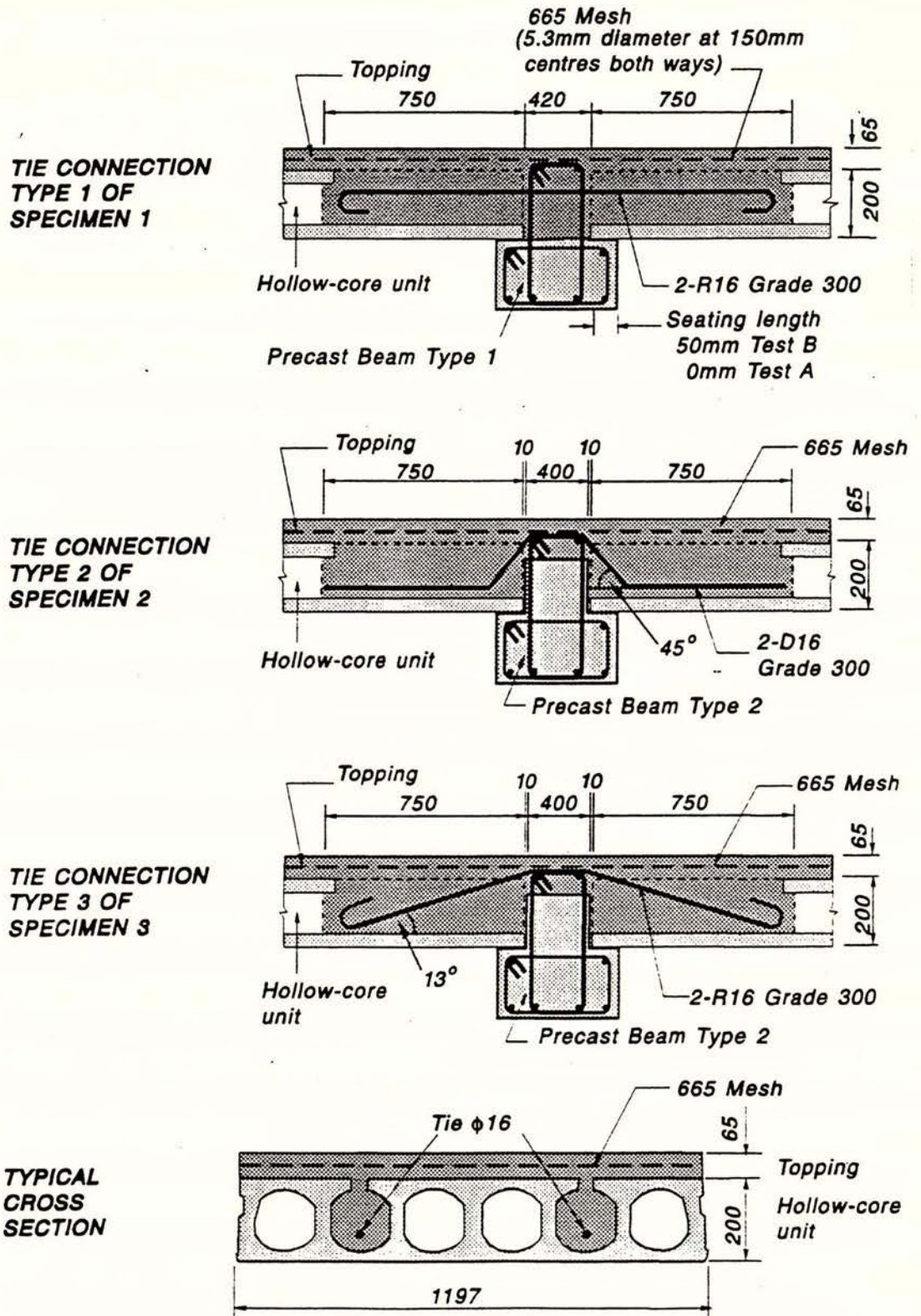


Fig 1.2: Tie connection details reported by Mejia and Park [6].

*Note: Connection Type 2 is not recommended for horizontal displacement loading.

Chapter 2.

Loss of Support through Axial Displacement

2.1 General

In the Loss of Support tests, a direct assessment was made of the strength and ductility of each particular detail by measuring the force-displacement relationships under axially applied loads. In each case, a statically applied gravity load was superimposed to place some emphasis on the ability of the detail to transfer shear forces to the supports.

For the purposes of establishing ductility performance, an axial displacement of 55mm was chosen as sufficient for the details examined. The choice of this figure was based on at least two independent factors. Firstly, the recommended seating length for prestressed slabs is 50mm, and therefore this is at least the distance that the unit must be moved to cause shear transfer by dowel action. An additional 5mm displacement was applied to discount the beneficial effects of aggregate interlock from the shear equation. For these reasons, this displacement value was used for the tests done by Mejia [6] when comparing the performance of recommended tie bar details. The second reason for a 55mm displacement is that the dilation of a single bay in a seismic load resisting frame has been estimated to be up to 60mm, therefore, it would seem that a displacement of the chosen magnitude is reasonable.

The displaced shape of a seismic load resisting frame (Fig 2.1) [3] illustrates the underlying mechanics of frame dilation. A cumulative displacement will occur along the support line of an exterior bay when expansion is due to a number of beam plastic hinges positioned within the span distance of the precast floor system. The magnitude of axial thrust accompanying these plastic hinge dilations is sufficient to overcome the restraint force provided by starter bars along the precast floor support line, and hence, loss of seating and eventual collapse is imminent.

The derivation of an equation for estimating frame dilation in seismic load resisting structures is presented in appendix A1 of "The Guidelines" [3]. Although some assumptions may be required regarding plastic hinge formation, the salient points are represented in this reference. The recommendations of appendix A1 with regard to the magnitude of dilation are described as tentative, as a good deal more research is required. What is true is that dilation of plastic hinges is a phenomenon that has been observed in many concrete research tests over the last 25 or more years.

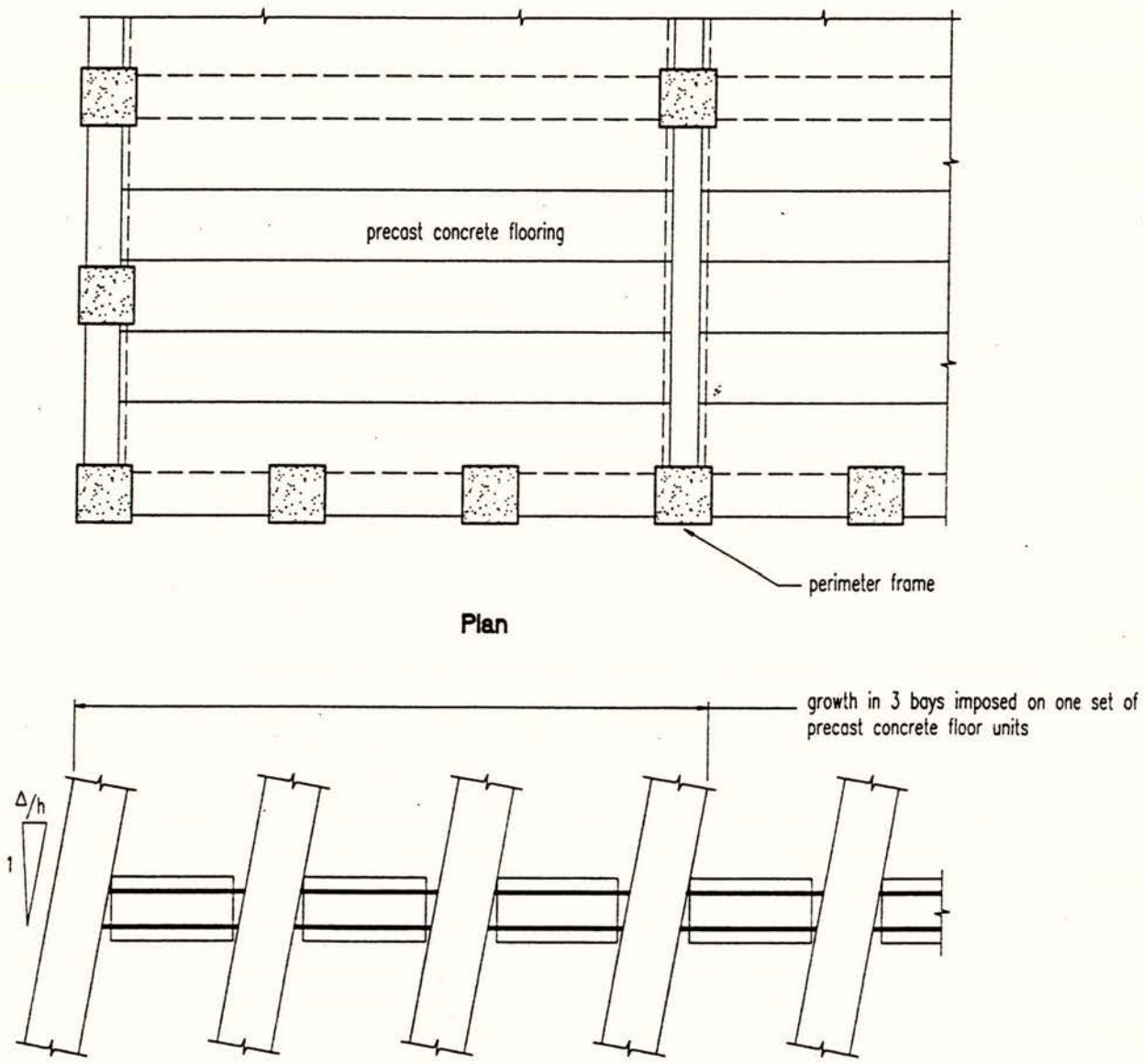


Fig 2.1: The expansion of a perimeter frame through sway displacements.

In each test, provided that the full horizontal displacement is achievable without fracturing the reinforcement, an additional vertical load is applied directly to the unit in order to determine the ultimate shear capacity of the support detail in an extended state. This vertical point load is additional to the self weight of the unit plus testing apparatus, as well as a superimposed dead load.

2.2 Description of the Test Rig

2.2.1 Horizontal Displacement (Fig. 2.2)

The horizontal force was applied to the test specimens via two parallel acting rams, each rated at 43 tons. These rams were attached directly to the support beam blocks, and hence the system was self stressing and had no reliance on external reactions. At the other end, the rams were each connected to a hinging carriage device that permitted both horizontal and rotational displacements. The Hollow Core unit was secured to the support carriages by two 310 UC 97 beams that were placed above and below the precast section, and bolted to it by eight 24mm diameter threaded rods. The threaded rods were made effective in shear by allowing the topping concrete to fill the Hollow Core voids for approximately 600mm from the end of the unit. Additional reinforcing was placed at the composite topping interface to develop the horizontal force through shear friction.

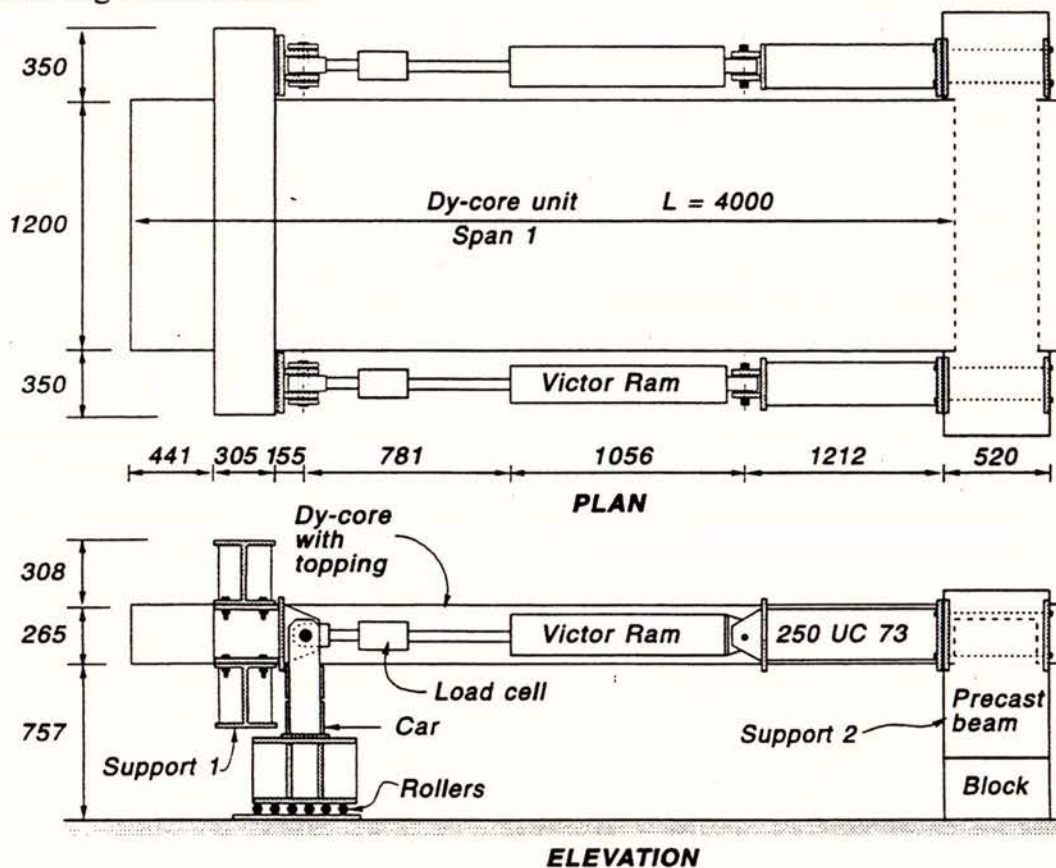


Fig 2.2: Method for horizontal loading.

2.2.2 Vertical Force (Fig. 2.3)

The provision for vertical force, in addition to unit self weight plus rig, was made available by the existing test apparatus used for support loss tests. This device utilises a 130 ton hydraulic ram acting through a series of spreader beams. The spreader beams were each seated onto a bedding of either plaster of Paris, or cement sand mortar where the steel contacted with concrete. A superimposed dead load of 3.25 kPa was provided over 60 % of the plan area of the unit by placing two layers of standard 40 kg cement bags. This load was present throughout all stages of testing, and represented a static floor service load reaction at the support equivalent to a U.D.L of 1.5 kPa.

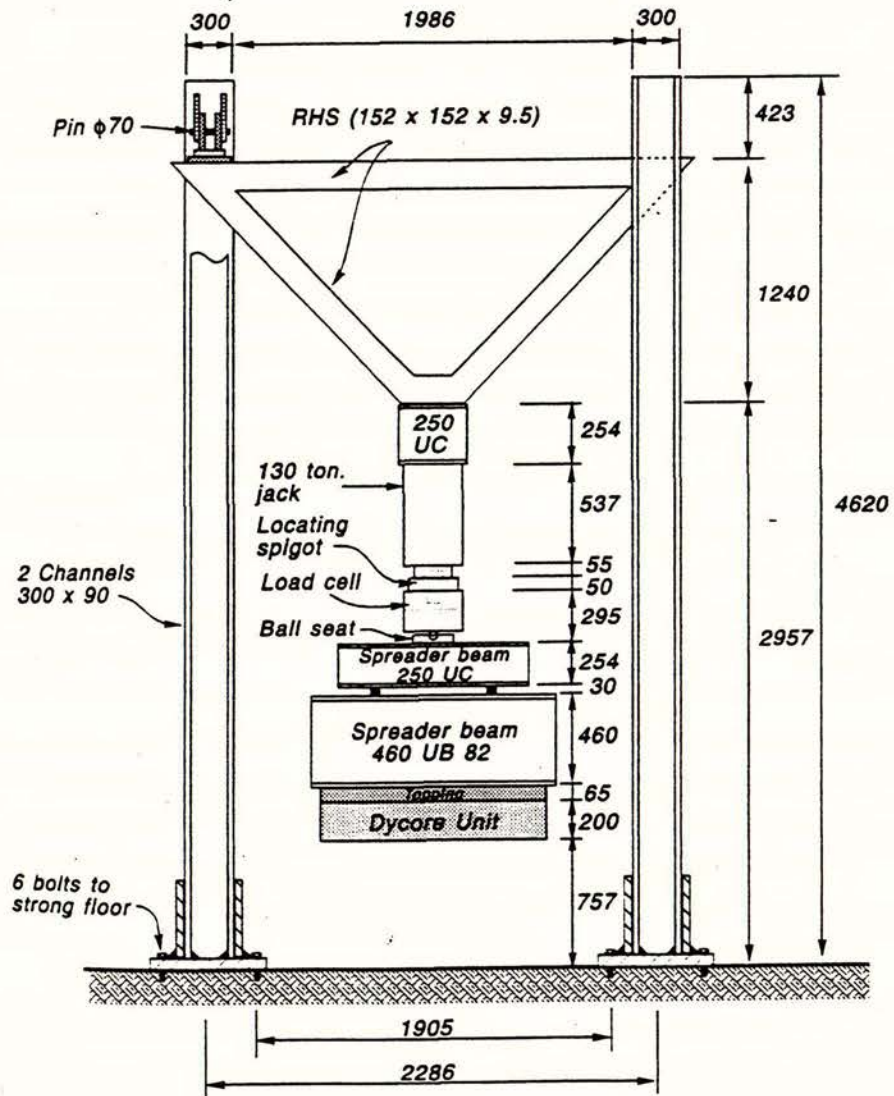


Fig 2.3: Method for vertical loading.

2.3 Instrumentation

2.3.1 Hydraulic Ram Forces

The two horizontal rams were each connected to a 44 ton load cell, positioned between the ram and the carriage device. Both load cells were connected to a data logger unit, with one ram additionally being connected to a strain indicator and plotter unit to provide an instantaneous "hard copy" of load vs displacement.

The vertical ram was connected to a 100 ton load cell that relayed to the data logger unit, a strain indicator and a load vs displacement plotter.

The load cell units were each calibrated before this series of tests on an Avery Universal Testing Machine.

2.3.2 External Displacements

Two 100mm potentiometers were connected between the floor and the Hollow Core unit near the support carriages to directly measure the horizontal movement of the unit away from the support. Two 300mm pots were connected to the Hollow Core unit at the support to measure vertical movements. In each test, three pots were placed on a station-to-target assembly to monitor the prospective displacement between the topping and precast unit near the support (Fig. 2.4).

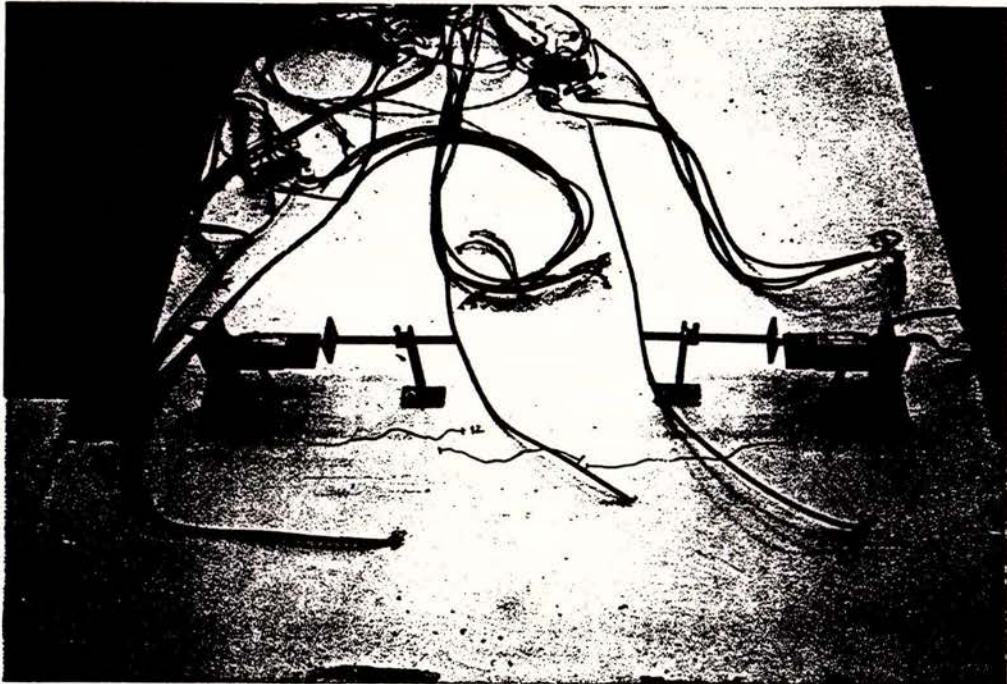


Fig 2.4: Potentiometer device for measuring topping slippage and delamination

Further potentiometers were placed on the concrete support block to monitor movement of the test rig in relation to the floor.

2.3.3 Bar Strains

Electrical Resistance Strain Gauges were connected to principal reinforcing to establish bar strain characteristics. Two types of gauge were employed, depending on the expected level of strain that would be attained by the bar element at a given section.

At the critical section, where the support line crack was expected to form, 20% strain gauges were attached. These gauges were supplied by Tokyo Sokki Kenkyujo Co, and were gauge type YL-5, 120Ω, of 5mm gauge length. Because of the sizeable strains involved, special adhesive was used that was recommended for use with large extension strain gauges, namely Armstrong A-12 epoxy. This adhesive was applied as a bedding for the gauge, and was then oven dried. Previous tests on this adhesive at the University of Canterbury showed that 19% extensions could be attained with the YL-5 gauge. At bar positions away from the critical section, ordinary 3% strain gauges were used. These were supplied by Tokyo Sokki Kenkyujo Co, gauge type FLA-5-11, 120Ω, of 5mm gauge length. Surface preparations and the method of fixing Electrical Resistance Strain Gauges were carried out in accordance of the departmental guidelines [8].

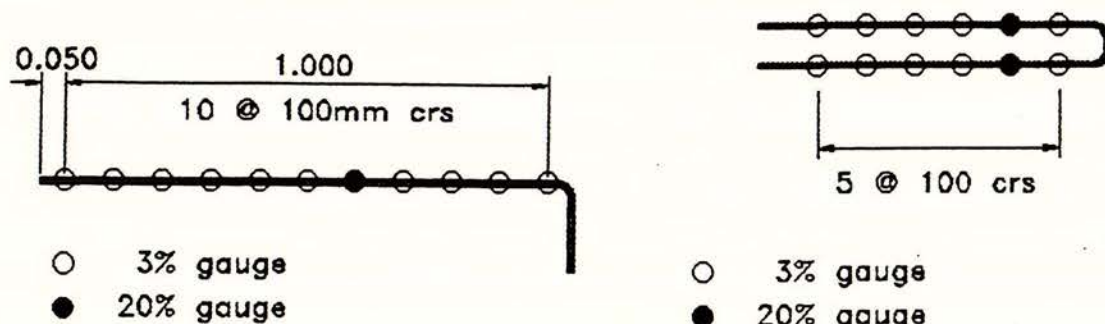


Fig. 2.5: Positions of strain gauges used in tests A and B

2.3.4 The Data Logger Unit

The load cells, potentiometers and strain gauges were all connected to the Metrabyte logger unit which converted voltage changes caused by linear displacements into digital values. These values were recorded against respective scan numbers as they were manually taken throughout the test. At the end of testing, the logged information was selected and converted into an ASCII file for use in any standard spreadsheet program.

Chapter 3.
Loss of Support: Test A

3.1 Description of Support Detail

This test examined a support detail that may be regarded as the standard adopted by structural designers throughout New Zealand (Figs. 3.1)

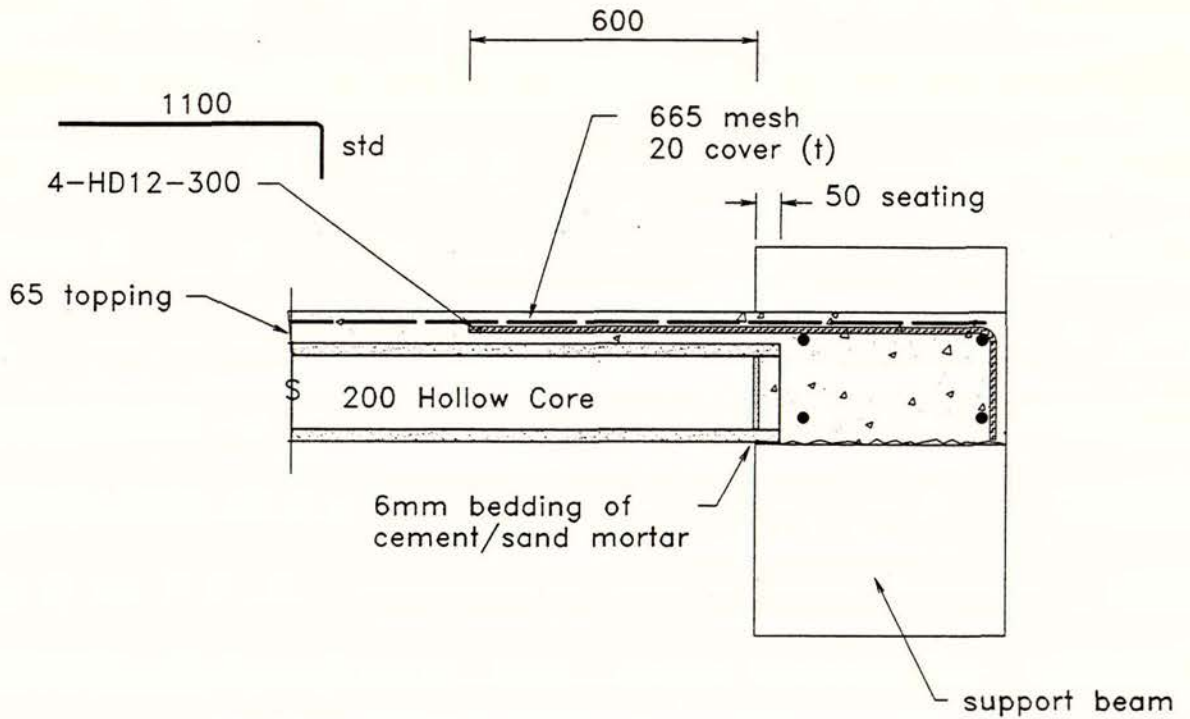


Fig. 3.1 a: Section, typical of support details.

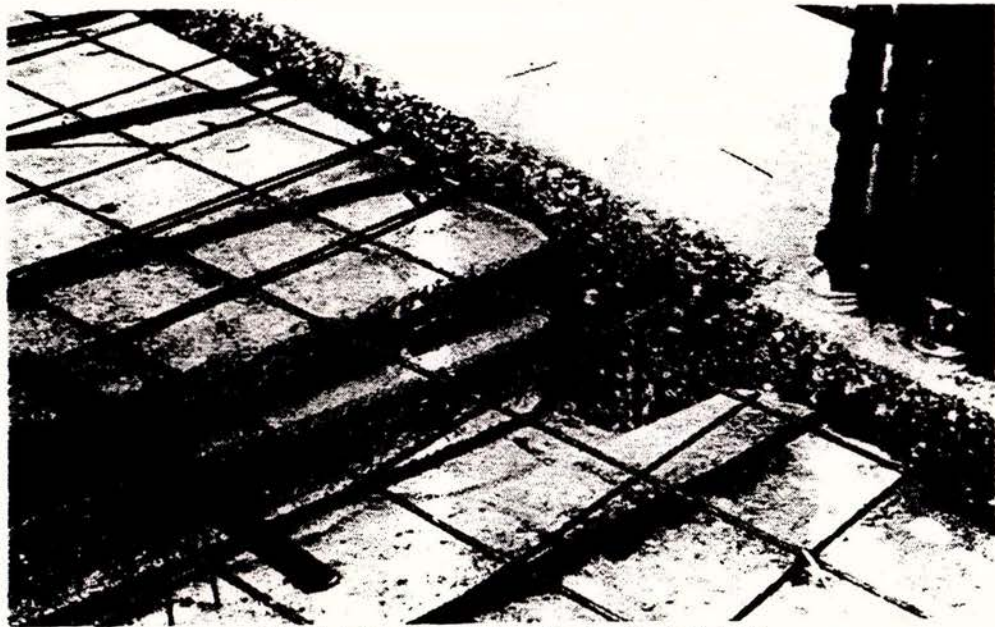


Fig 3.1 b: Example of a typical detail

The mechanics of this detail are based on the assumption that sufficient horizontal shear strength can be developed between the top of the precast unit and the composite topping to transfer diaphragm shear actions. In the advent of dilatational type loadings, the shear strength developed at the composite section interface is required to match the overstrength axial restraint capacity of the projecting starter bars. Section eight of NZS 3101: 1982 "The Design of Reinforced Concrete Structures" [1] specifies that the maximum horizontal shear stress that may be developed between clean, intentionally roughened surfaces without shear connectors is 0.55 MPa. Therefore, for 12mm diameter grade 430 starters placed at 300mm centres, a projection of 600mm into the topping would be sufficient to develop the full reinforcing tensile capacity through horizontal shear. By allowing a strain hardening factor of 1.4 and a bar bond region of at least 150mm from the point of bar curtailment, the maximum required interface shear stress along the support line is:

$$v_h = \frac{f_{su} A_b}{\phi s l_d} = \frac{1.4 \cdot 430 \cdot 113}{0.75 \cdot 300 \cdot 600} = 0.5 \text{ MPa}, \dots < 0.55 \text{ MPa}. \quad (3.1)$$

The contribution of temperature and shrinkage reinforcement, usually in the form of wire fabric, does not need to be considered in this equation because it is continuous throughout the topping, and therefore its strength development does not depend of this mechanism.

This detail may be made continuous when flooring units are supported on both sides of the support element, Fig 3.2:

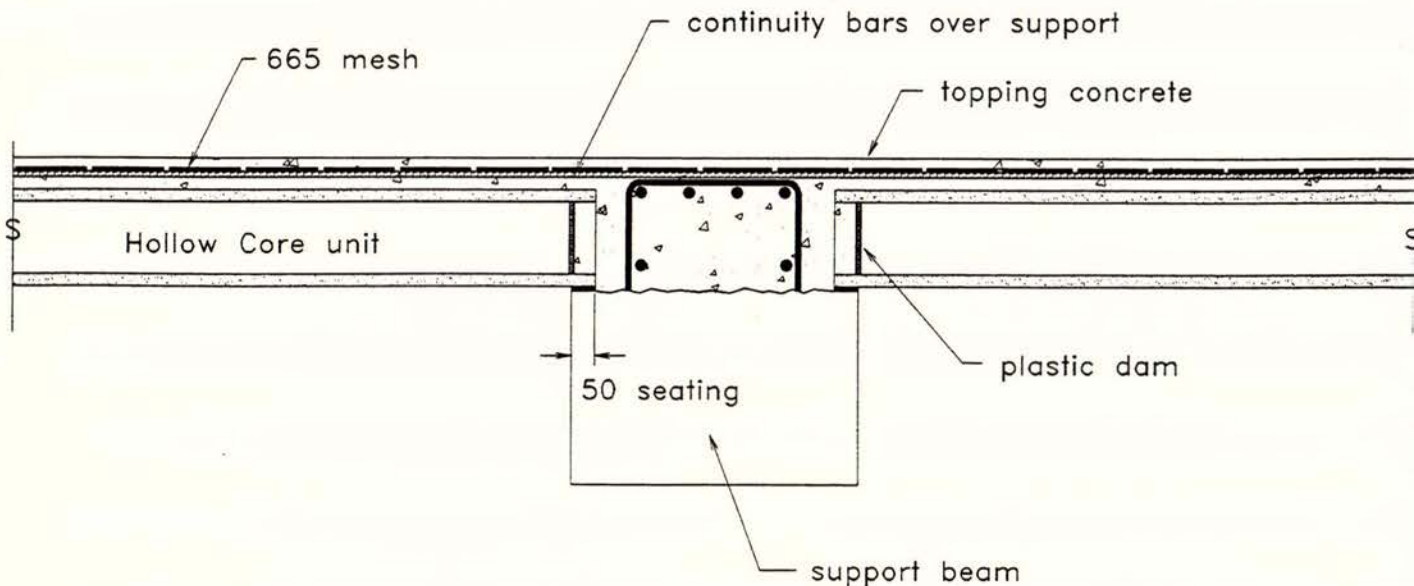


Fig 3.2: Continuity over supports

Continuity bars are often detailed to serve a dual purpose by developing both negative moment bending capacity at the supports under gravity loads, and shear friction for diaphragm actions under lateral frame loads. The selected size and spacing of continuity and starter bars depends on the a variety of factors, the eventual configuration of top steel in this case may be governed by either design parameter.

Regardless of whether the top steel is designed as starters only and is not included in flexural calculations, this reinforcing will provide some negative moment capacity. The actual magnitude of negative moment that can be developed is proportional to the effective depth of the composite section, and is influenced by the rotational stiffness of the support element. The bar bond development length of starters would generally not be of concern, however, the bond surface between the composite topping and precast unit beneath the starters will need to be considered, as described in the denominator term of eqn. 3.1. For these reasons, the length of starter bars should not fall below a value that allows for the full transfer of horizontal shear between the topping and precast unit, with a margin for bar embedment beyond the critical length.

Where continuity bars are included as part of the flexural calculations, the point of inflection will need to be considered, as per the requirements of section 5.3.24 of the concrete design code [1].

3.2 The Detail Tested

Test A was constructed as follows:

precast unit	topping	G430 starters	starter length	mesh
200mm H.Core	65mm	4-HD12 @ 300 crs	600mm	665 (5.3mm)

For this test, the 665 mesh component was carried over into the support member. Although this is generally not recommended construction practice, it is common place on many construction drawings. The mesh was also carried over into the supports in the tests conducted by Mejia [6], and therefore was included likewise in this test as a comparison.

3.3 Materials

3.3.1 Concrete

For the topping concrete, a design strength of 35 MPa was used in order to achieve an insitu crushing strength greater than 25 MPa in a comparatively short period. Although it is

possible to achieve the design strength in seven days with continual wet curing, this duration is unrealistic for most practical applications. Ideal moist curing is lacking on most building sites, therefore, it was opted to order a higher grade of concrete and allow only three days of curing using damp hessian cloth. The ordered concrete mix:

design strength	max. aggregate	ordered slump
35 MPa @ 28 days	13mm	100mm

Considerable difficulties surrounded the supply of concrete at a specified slump of 100mm. The initial delivery was measured at 160mm, and was rejected as being outside the snatch sample upper tolerance value of 140mm. The replacement delivery was measured at 60mm, and was accepted as being just on the minimum tolerance level of 60mm. Although this concrete was within tolerance and accepted for this test specimen, it may have been "turned around" by a contractor because of its reduced workability. The topping concrete properties were as follows:

slump received	test insitu strength
60mm	38 MPa @ 23 days

3.3.2 Reinforcing Steel

Tensile tests were performed on the 12mm diameter grade 430 bars and the 665 wire mesh. Measurements were also made of the total elongation of each test specimen at fracture:

taken over three specimens:	avg. yield stress	avg. UTS	avg. ϵ_{sh}	avg. strain at UTS	avg. strain at fracture
HD12 bar	445 MPa	613 MPa	1.35%	12.74%	20.9%

avg. E = 205 GPa

taken over three specimens:	avg. proportional limit	avg. UTS	avg. strain at fracture
665 mesh	528 MPa	660 MPa	5.4%

avg. E = 196 GPa

For the hard drawn wire specimens, the maximum and minimum elongation's measured at fracture were 6.4% and 4.1% respectively.

3.4 Results of Test

The outcome of test A is graphically portrayed in Figs 3.3.

The initial response to loading produced little movement, with a displacement of only 0.27mm at the peak horizontal load of 352 kN. The first cracks appeared across the topping above the end of the Hollow Core unit at a load of 250 kN, with an maximum topping crack width at the peak load level of approximately 0.4mm.

At 352 kN, a sudden fracture took place through the end of the precast Hollow Core section. This resulted in a major crack 0.6mm wide occurring through the topping 650mm from the face of the support beam, beyond the point of starter bar curtailment. From here the nature of the test changed completely. The horizontal force dropped to 130 kN, and reached a post fracture maximum of 178 kN at a displacement of 5mm. The force requirement decreased steadily out to a displacement of 18mm, with intermittent fracturing of mesh wire throughout this phase. Once the contribution of the topping mesh was completely lost, only residual sliding friction forces acted against the rams.

It was obvious that a complete loss of bond had occurred between the topping and precast concrete, with a vertical separation of 4mm between these elements at 18mm of displacement. At a displacement of 25mm, the soffit of the Hollow Core unit had dropped below the support level by 7mm, at a displacement of 32mm this value had increased to 12mm. The test terminated when the Hollow Core unit fell off the support at a displacement of 43mm.

Although all the topping mesh fractured during the test, not all the wires fractured within the space of the principal topping crack. Three wires fractured a short distance inside the topping adjacent to the crack surface, and these wires supported the unit in a catenary fashion. This support action tended to peel the topping away from the Hollow Core unit on the mid-span side of the principal crack.

3.5 Analysis of Test Results

Probably the best initial approach to analysing test A is simply to trace the progress of the load-displacement diagram (Fig 3.3 a). This curve can be divided into four distinct regions that characterise the structural response during the test (Fig 3.3 b). Each of these regions indicate a basic change in the resistance mechanism against the imposed horizontal displacement, and the diagram as a whole clearly indicates the respective differing contributions of the concrete and steel components.

Load-Displacement (Test A)

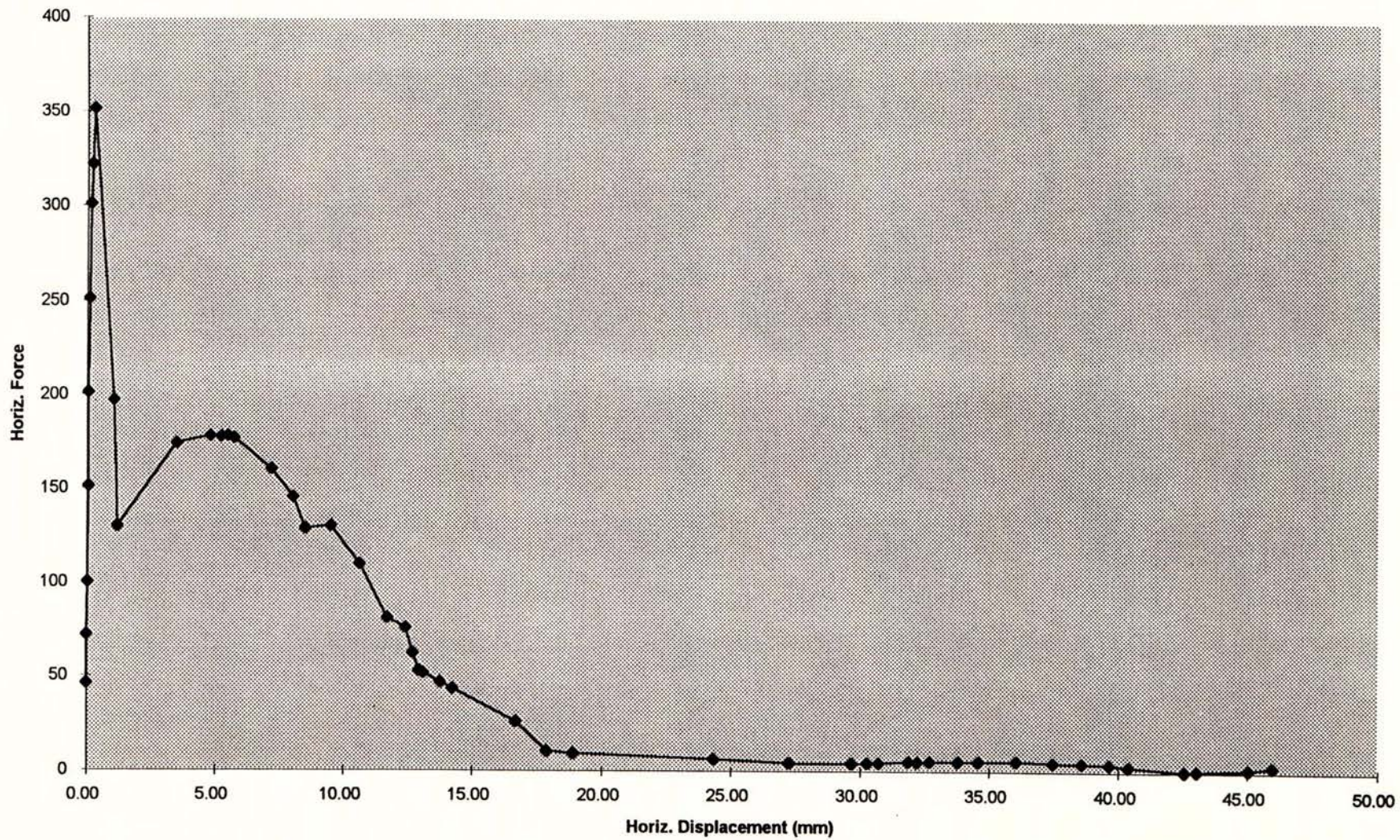


Fig. 3.3 a: Load-Displacement diagram for Test A

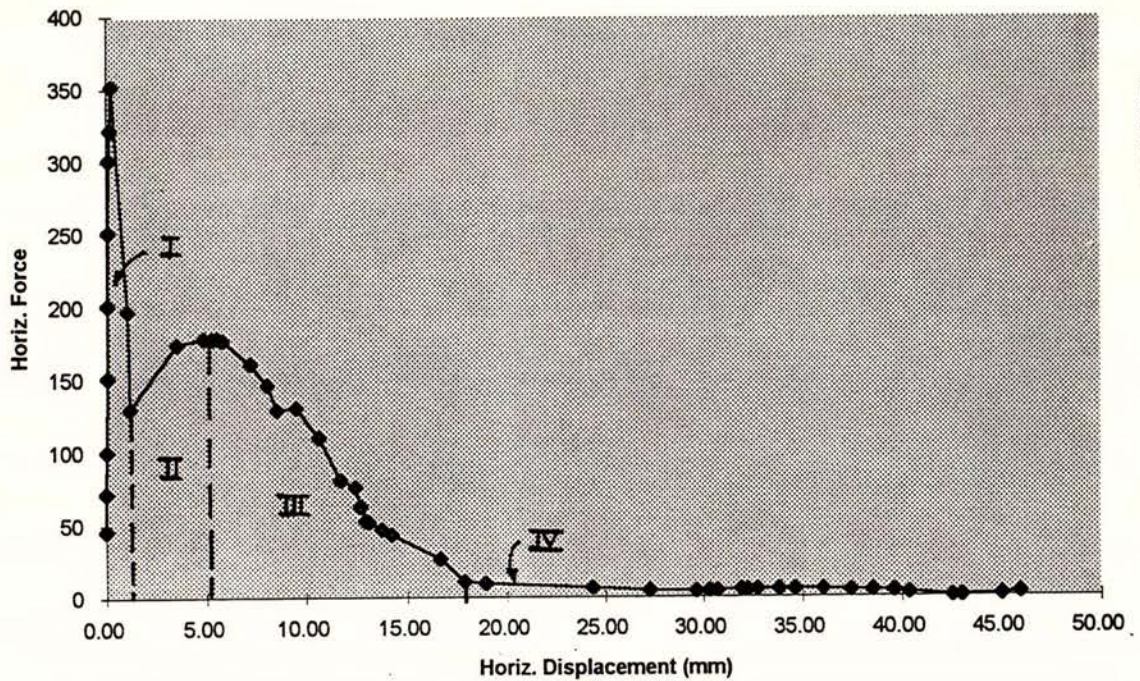


Fig. 3.3 b: Load-Displacement curve divided into regions of significance

(I) Peak Load and Fracture

The initial response showed a stiffness of 1825 kN/mm, with resistance being provided by the entire composite section. At 300 kN (85% of peak load), only 0.14mm of horizontal movement was registered on the displacement potentiometers, with topping cracks appearing across the entire unit above the interface of the Hollow Core unit and the insitu beam concrete.

Initial cracking had appeared at approximately 250 kN and the effect of this on the proportion of load carried by reinforcing is illustrated in Fig. 3.4 a, which shows a marked increase in steel force at this load level. As displacement increased beyond 0.1mm, the steel contribution to resistance increased, but at a sharply decreasing rate. In other words, the steel was proving not to be the primary stiff element that would resist the total force, and at peak load contributed only 28% of the total reaction.

With the total horizontal force as the upper line (Fig 3.4 b), and the steel force (starters plus mesh) across the support region as the lower line, the proportion of load carried by the concrete is the difference between the two lines. The deduced value is almost constant at 250 kN up to fracture at 0.27mm displacement. This implies that the concrete section was mobilised, showing increased displacement for no increase in load. However, the small displacements involved would have not been sufficient to overcome the post cracking tensile strength of the infill concrete around the Hollow Core voids, and the influence of edge effects caused by wedging between the sides of the precast unit and support block was becoming prominent. The

combined result is a tendency of increasing total stiffness in the system immediately prior to fracture (Fig. 3.4 b).

Proportion of Steel Force in Section up to Fracture Displacement (0.27mm)

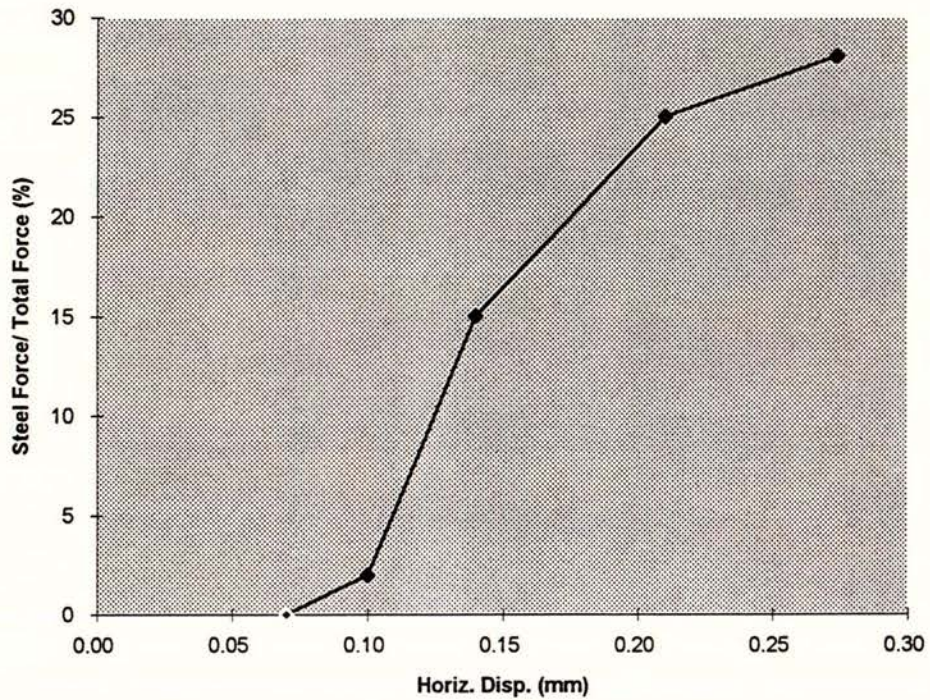


Fig. 3.4 a: Proportion of total horizontal force resisted by starters and mesh over the support region prior to fracture

Total Force & Steel Force at Displacement for Region I

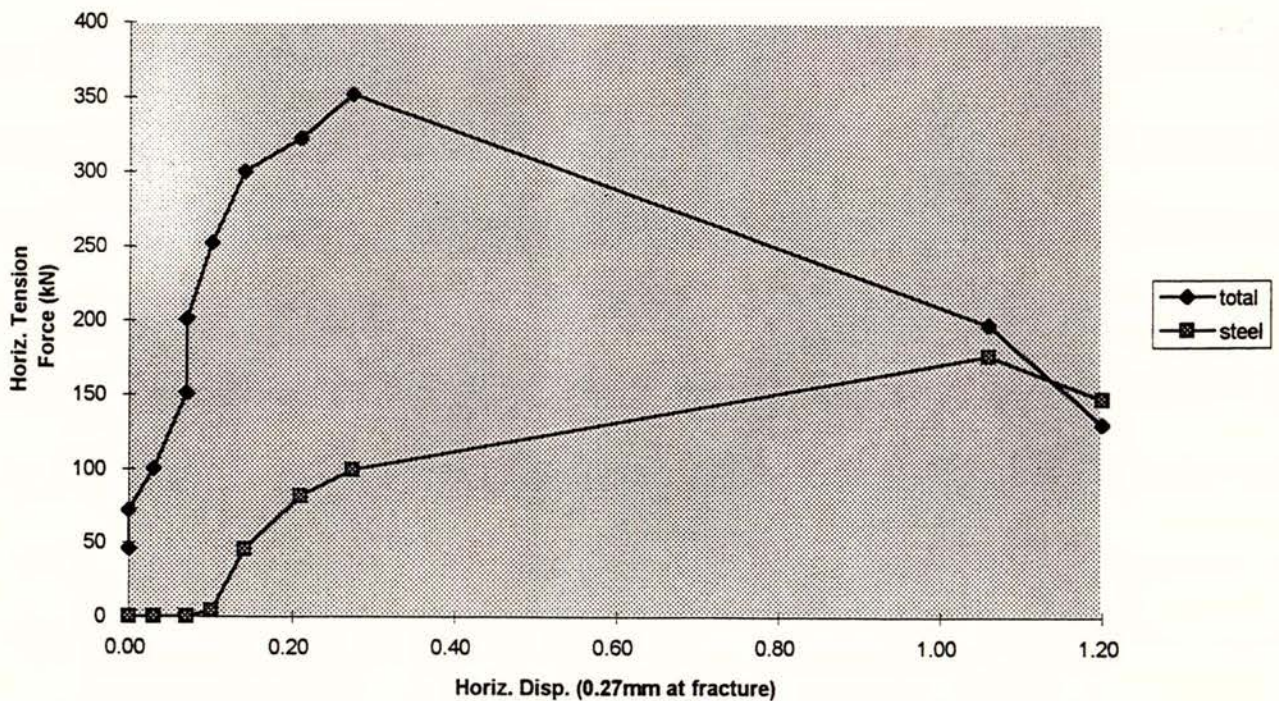


Fig 3.4 b: Total force and Steel force (starters and mesh) over the support region

The individual behaviour of the starter bar and mesh wire elements are tabulated:

	avg. stress & disp. before fracture	proportion of total reaction	avg. stress & disp. after fracture	proportion of total reaction
HD12 starters	134 MPa at 0.27mm	17%	253 MPa at 1.06mm	58%
665 mesh	216 MPa at 0.27mm	11%	350 MPa at 1.06mm	31%
		Σ 28%		Σ 89%

The maximum starter bar stress at this stage of the test was less than 60% of the nominal yield stress, and the maximum stress for the mesh was 73% of the nominal proportional limit. The fact that neither the starters or mesh reached their proportional limits is illustrated in Figs. 3.5 a and 3.5 b, and in the post-fracture section, the steel forces decrease in proportion to the loads of 197 kN at 1.06mm down to 130 kN at 1.15mm displacement. These diagrams are direct measurements of the bar stresses at stations along these elements, as deduced from electrical strain gauge readings. The diagrams describe average values taken over two bars and two mesh wires. The characteristic magnitudes and distribution of stress along the starter bars and mesh showed little variance and therefore representation by average values is justified.

The starter bar diagram 3.5 a indicates a sudden increase in stress at station No. 9, and this is due to a sizeable crack that formed across the topping at this point when the unit fractured. Evidence that this crack was forming is indicated by the slight increase in stress at this point immediately prior to fracture.

The diagram also suggests that the bar bond efficiency was greater in the insitu beam concrete than on the topping slab, as indicated by the respective slopes on either side of the support line crack at station No. 5.

The strength development of the respective starters and mesh elements was not in proportion to the area of each. The area of HD12 starters was 452mm² (72% topping the steel area), and the area of mesh was 176mm² (28% of topping steel area). In the pre-fracture section, the mesh developed 40% of the total steel reaction, decreasing to 35% of the total steel reaction after fracture. It can be seen that the mesh developed proportionally greater stresses than the starters, and this is due to the differing bond efficiencies of each of these element at small displacements.

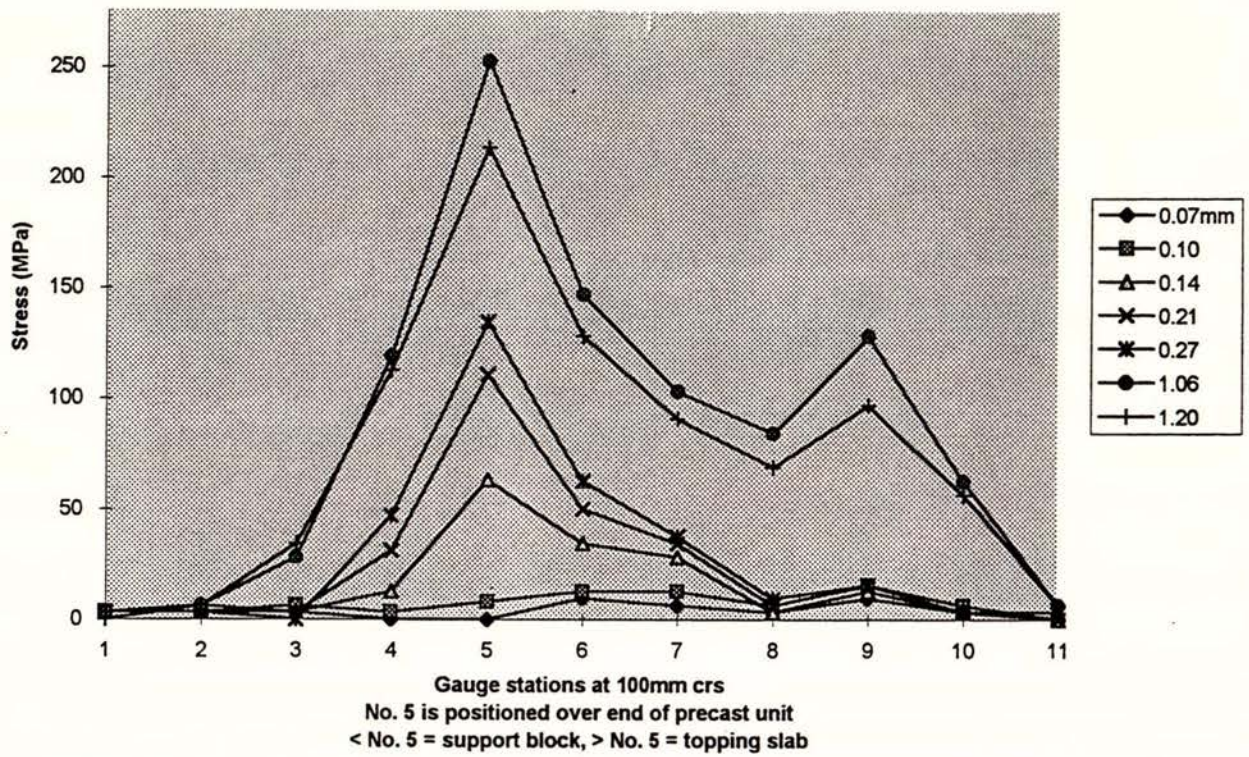


Fig 3.5 a: Avg. stress distribution along HD12 starter bars at stage I of test

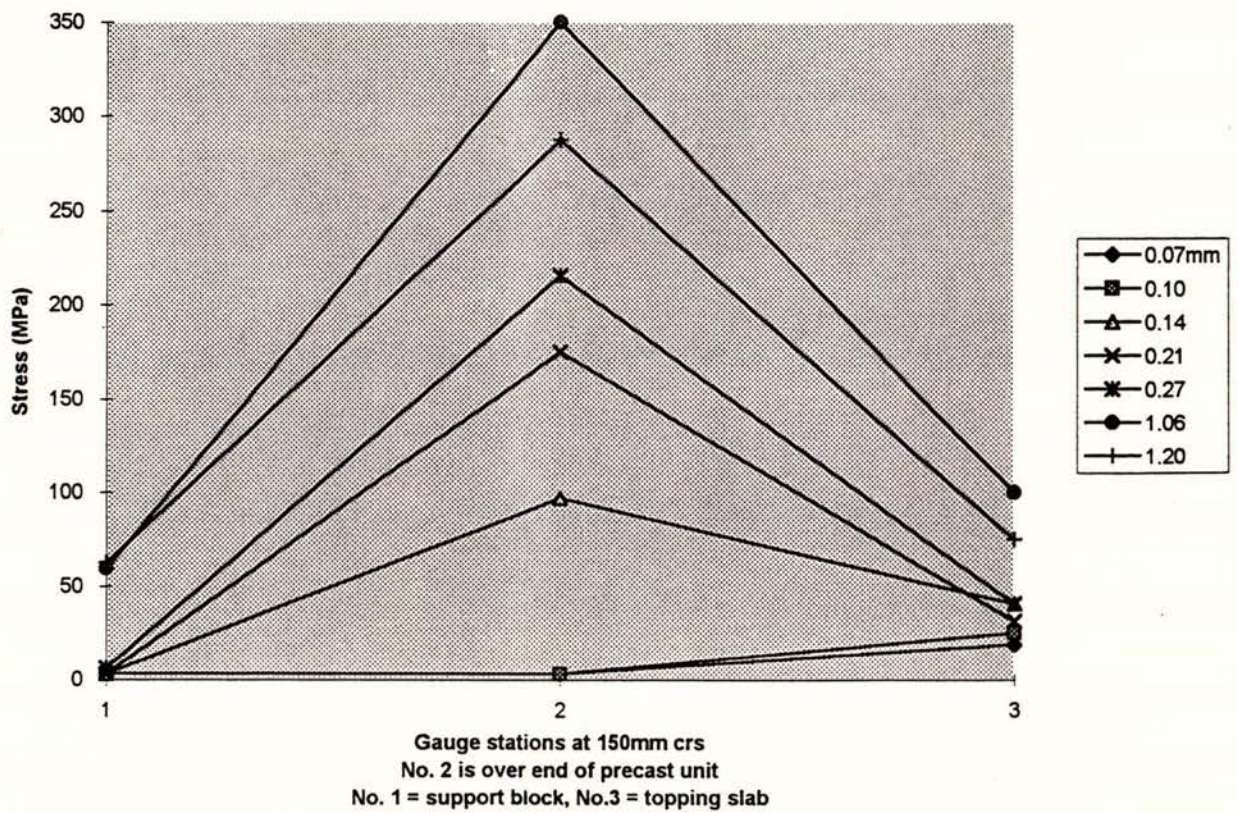


Fig 3.5 b: Avg. stress distribution in mesh over support region at stage I of test

The fracture of the Hollow Core unit resulted in two principal cracks, generally extending through the entire section of the unit and mostly occurring along the face of the support. The cracks started near the termination point of the concrete support block at the edges of the unit, and angled inward toward the centre line of the unit (Fig. 3.6). This suggests the influence of shear stresses between the support block and the Hollow Core unit, provided by the topping concrete forming a 50mm long mortar joint on each side of the precast unit.

The crack width in the precast unit corresponded directly with the measured test rig horizontal displacement of approximately 1mm.



Fig 3.6: Soffit of Hollow Core unit after fracture

(II) Post-Fracture to Post-Fracture Peak Load

From the position at post fracture, further displacement resulted in an increase of reaction up to the post-fracture peak load of 178 kN, one half of the test peak load. Through this stage of the test, the applied horizontal force was resisted by a combination of mechanisms. Though it was clear that complete separation had occurred between the Hollow Core unit and the support, prestressing strands were still embedded, especially near the edges of the unit, where the maximum embedment length was measured at 60mm. The effect of bond between these stubs of strand and the restrained section of the Hollow Core unit would have contributed to the post-fracture reaction, as would to a lesser effect the friction between the unit, the topping slab and the support.

The maximum load that could be developed by steel reinforcing at this stage was entirely dependent on the mesh wire across the principal topping crack, 650mm from the face of the support. Assuming that the mesh wire was at peak stress of 660 MPa, the maximum contribution of reinforcing steel was in the vicinity of 116 kN, 65% of the post-fracture peak load.

The maximum starter bar stress that was registered during the test occurred over the support line of the Hollow Core unit at the post-fracture peak load, and was 316 MPa at a displacement of 5.5mm. The maximum mesh wire stress over the support region was 338 MPa, less than 375 MPa recorded in stage I of the test. Fig 3.7 a shows the average starter bar stress distribution at the peak post-fracture load. Figs 3.7 b & c illustrate a curve fit of the bar stress profile.

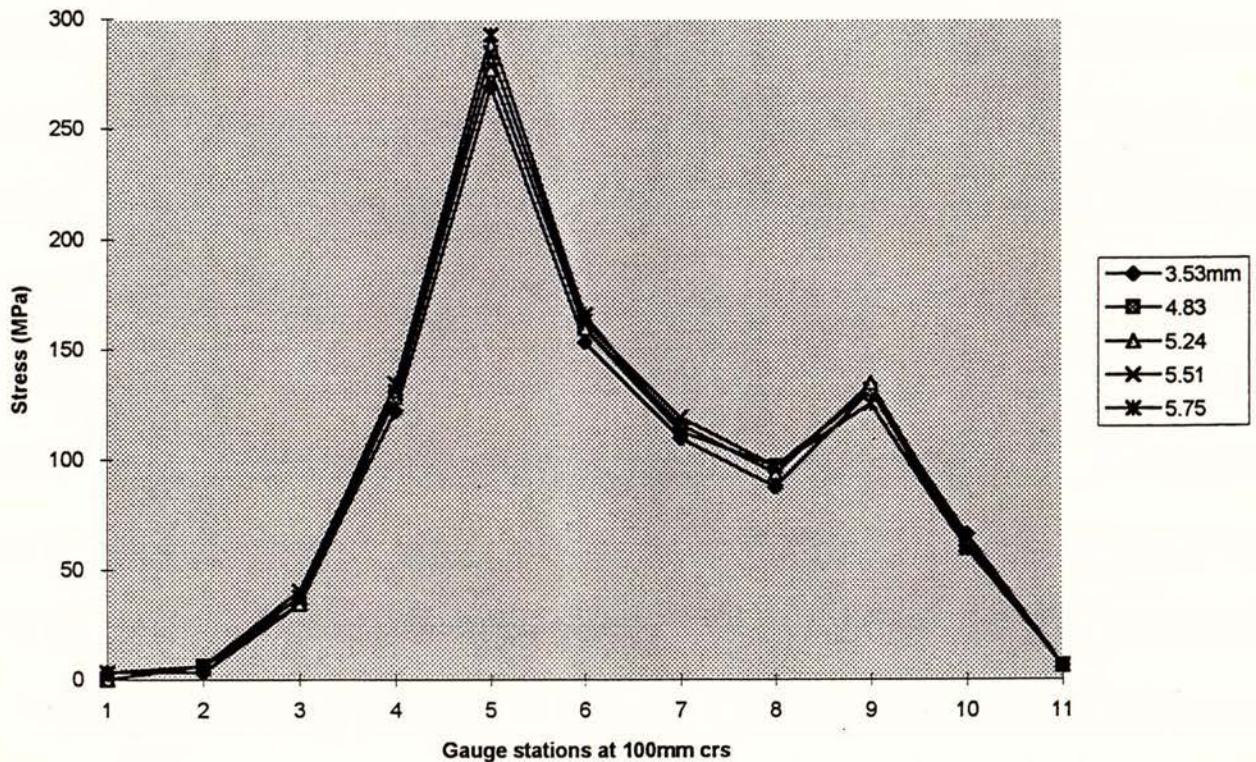


Fig. 3.7 a: Avg. stress distribution along starter bars up to post-fracture peak load

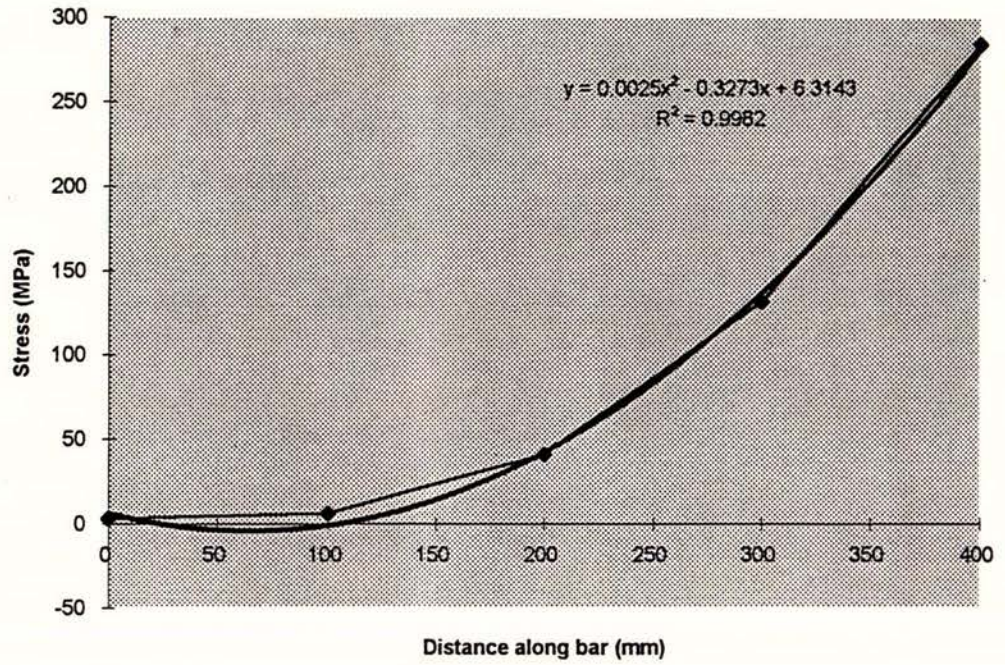


Fig 3.7 b: Fitted curve of starter bar stress distribution over the support block at post-fracture peak load

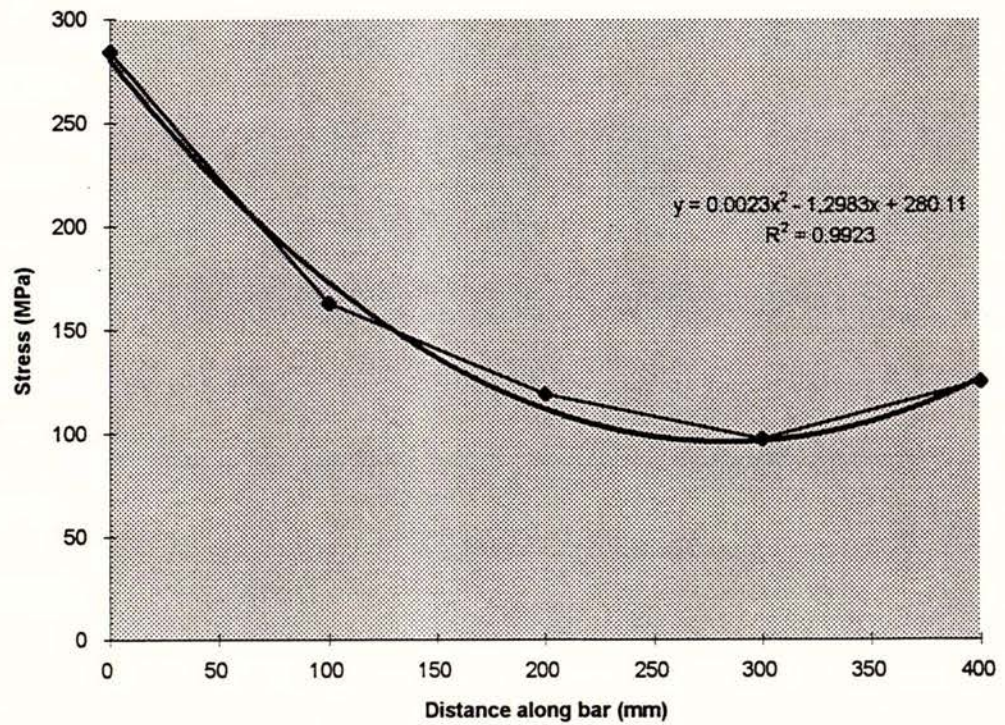


Fig 3.7 c: Fitted curve of starter bar stress distribution into the topping slab at post-fracture peak load

Figs 3.7 b & c indicate a strong correlation between the measured stress distribution calculated from strain gauge readings and the fitted parabolas. This would indicate a linear variation of bond stress along the bars under this level of bar stress. The fitted equation for the bar stress for the embedment length over the support block is:

$$f_s = 0.0025x^2 - 0.33x + 6.3 \quad (3.2 a)$$

Likewise, the fitted equation for bar stress into the topping slab is:

$$f_s = 0.0023x^2 - 1.3x + 280 \quad (3.2 b)$$

Because the bond stress may be expressed as:

$$u = \frac{d_b}{4} \cdot \frac{df_s}{dx} \quad (3.3)$$

The bond stress along the bar for both cases is:

$$(a) \text{ embedment over the support block} \quad u = 0.015x - 1 \quad 0 < x \leq 400\text{mm} \quad (3.4 a)$$

$$(b) \text{ embedment into the topping slab} \quad u = 0.014x - 3.9 \quad 0 < x \leq 400\text{mm} \quad (3.4 b)$$

From these equations, the maximum calculated bond stress at gauge no.5 from eqn. 3.4 a with $x = 400\text{mm}$ is 5 MPa. The maximum bond stress at gauge no.5 from eqn. 3.4 b with $x = 0\text{mm}$ is -3.9 MPa, the negative sign indicating the direction at which the bond stress acts. These values of bond stress indicate adequate starter development for the given conditions of bar stress and adjacent concrete cover [10].

(III) Post-Fracture Peak Load to Full Loss of Reaction

Once the peak load displacement of 5.5mm was exceeded, a steady loss of reaction occurred as the mesh wires serially fractured, and the residual bond and friction effects were overcome. At 18mm displacement, the horizontal reaction was reduced to only a nominal value caused by sliding friction between the unit Hollow Core unit and the seating and three mesh wires that had fractured within the topping. The mesh wires only resisted residual pullout forces and therefore, this is effectively the point where the contribution of reinforcing steel was lost.

Notable separation had occurred between the Hollow Core unit and the topping. Measurable reaction from composite bond had probably been lost early during this stage of the test, when the separation of these elements initiated.

(IV) Loss of Reaction to Failure

Although the reaction forces were removed from the system, the final stage of the test would reveal the point at which the floor element collapsed. This stage was characterised by increasing separation between the Hollow Core unit and the topping. At 25mm displacement, the unit had slipped 7mm below the level of the support block, and was supported primarily by dowel action provided by the prestressing strand stubs which protruded from the fractured section. Spalling also occurred along the seating line of the support block at this displacement. At 43mm displacement, the support through dowel action was overcome and the unit fell off the support. At failure the topping separation had increased to a maximum of 15mm



Fig 3.8: Soffit of Hollow Core unit showing fracture at support

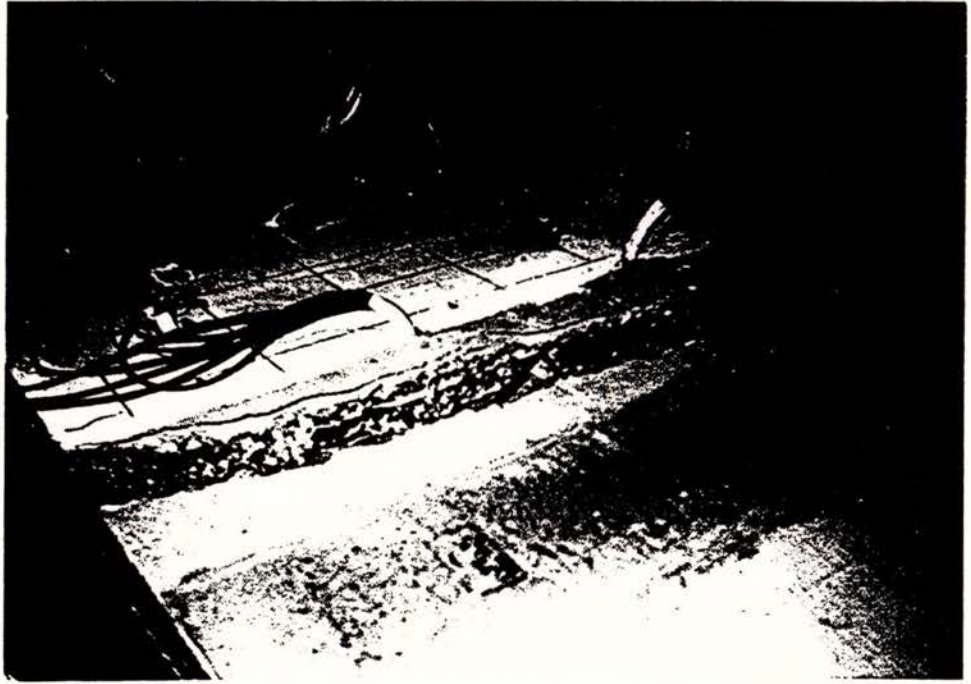


Fig 3.9: Principal topping crack separation just prior to collapse

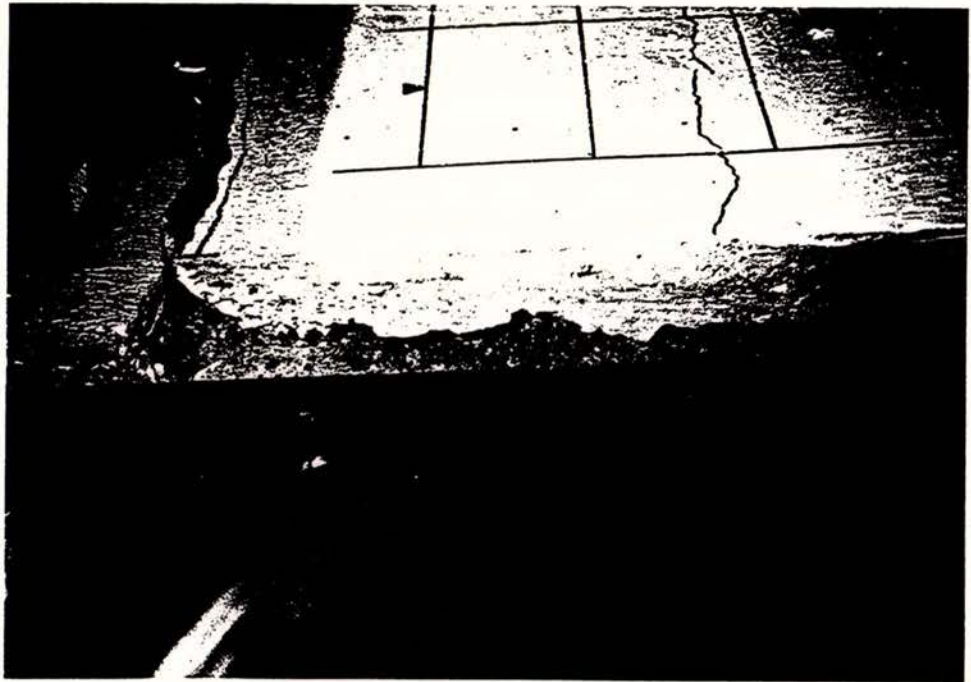


Fig 3.10: Topping separation caused by downward slippage of the Hollow Core unit



Fig 3.11: Fractured Hollow Core section after removal

Note that the plastic dams are still intact in the outer two voids, and this occurred symmetrically about the unit centre line. Also note spalling along the support line.

3.6 General Analysis

3.6.1 Fracture of the Hollow Core unit at the Support

Before the fracture occurred, topping cracks over the support region had opened to about 0.4mm, and therefore, the contribution of the residual tensile strength of this concrete may have been comparatively small. If we then assume that the total load was resisted by the topping steel and precast section only, we find that the Hollow Core component failed under a surprisingly small axial tensile stress of:

$$f_{\alpha} = \frac{P_{pc}}{A_{pc}} = \frac{253 \text{ kN}}{0.119 \text{ m}^2} = 2.1 \text{ MPa} \quad (3.5)$$

Eqn. 3.5 alone, however, is too simplistic because it does not include the contribution of shear stresses caused by the edge effects between the precast unit and the support block. A fuller approach would be to estimate the magnitude of shear stress between the infill topping and the side of the Hollow Core unit, and then include this in an equation for principal tensile stress. References containing information on concrete interface shear for specific surface

conditions and slip at the interface [9,10] indicate that an interface shear stress of at least 1.5 MPa should be obtainable in this situation. For an element with combined monoaxial and shear stress, the equation for the principal tensile stress is:

$$f_t' = \frac{f_{\alpha}}{2} + \sqrt{\left(\frac{f_{\alpha}}{2}\right)^2 + v^2} \quad (3.6)$$

and the principal stress plane is located, relative to the plane of axial stress as:

$$\theta_p = \frac{1}{2} \tan^{-1} \left(\frac{2v}{f_{\alpha}} \right) \quad (3.7)$$

Substituting the values of the respective axial and shear stresses of 2.1 MPa and 1.5 MPa into eqns. 3.6 and 3.7 yields:

$$\begin{aligned} f_t' &= 2.9 \text{ MPa} \\ \theta_p &= 27.5^\circ \end{aligned}$$

Generally, the principal tensile stress should not exceed a value of $0.33\sqrt{f_c'}$, which for 45 MPa concrete becomes 2.2 MPa. This figure is easily exceeded, and it therefore appears that the effect of side restraint could strongly influence the behaviour of Hollow Core slab ends under this type of loading. We must also bear in mind that a conservatively low value was chosen for the potential mortar joint shear stress in this example. The beneficial effect of axial compression through prestress force would be of small consequence near the end of the Hollow Core unit.

The ACI recommended equation for principal tensile stress of $0.33\sqrt{f_c'}$ is substantiated by tests [11], therefore, we can predict the orientation of the fracture plane by rearranging eqns. 3.6 and combining:

$$\theta_p = \frac{1}{2} \tan^{-1} \frac{2 \cdot \sqrt{\left(0.33\sqrt{f_c'} - \frac{f_{\alpha}}{2}\right)^2 - \left(\frac{f_{\alpha}}{2}\right)^2}}{f_{\alpha}} \quad (3.8)$$

Substituting the appropriate values of 45 MPa and 2.1 MPa into eqn. 3.8 yields:

$$\theta_p = 12.7^\circ$$

The actual failure planes of the test unit are shown in Fig. 3.12 a, and the orientation of these planes, caused by shear and tension interaction at the support, are about 13° and 9° to the axis of the unit. It can be seen that fracture occurred through the entire section of the unit except a small portion at the central web, measuring 30mm (web width) wide by 40mm (Fig. 3.12 b).



Fig 3.12 a: Plan of fractured end of Hollow Core unit

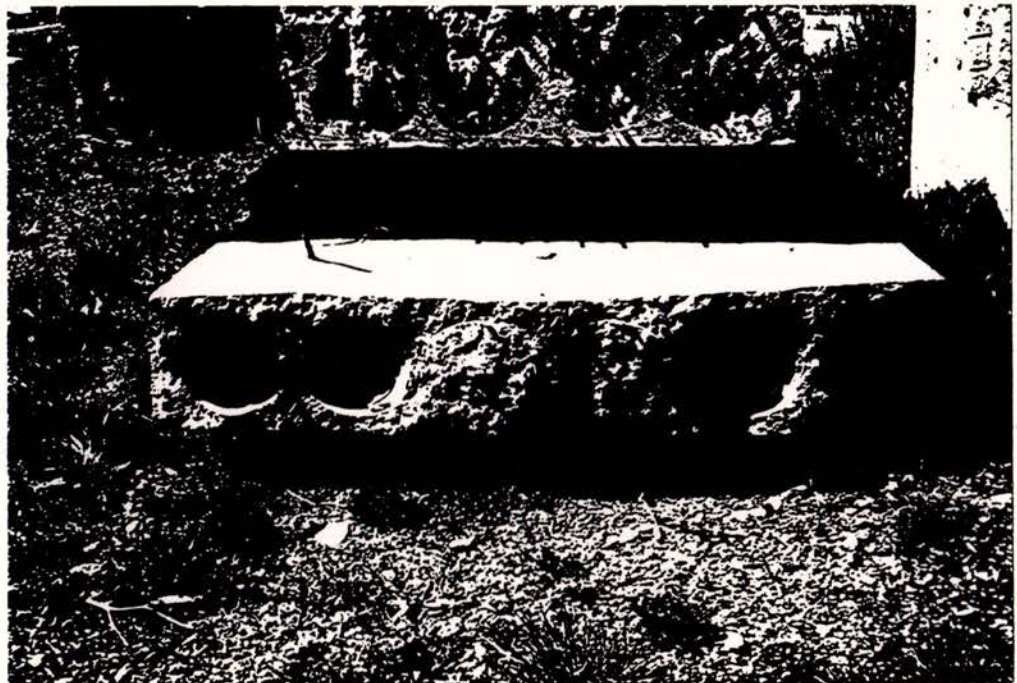


Fig 3.12 b: End view of fractured section

3.6.2 Work Done

The conservation of energy principal requires that the sum of the *external* work done on a structure by applied loads (or displacements) must equal the sum of the *internal* work done by the structure in resisting these loads. Because the term work is defined as the product of a force acting over a distance, the quantity of work is normally derived as a summation of the displaced response of a structure under an externally applied load. The bracketed term displacement has been incorporated in the above description of external work because for a seismic load resisting structure it is equally true that the internal work done by the structure is caused in response to externally applied displacements (ie, the ground movement at foundation level).

The external work done on the detail tested is the summation of the area under the load-displacement curve (Figs. 3.3). The internal strain energy in this detail was primarily conservative (ie, recoverable) up to the extent that the section remained elastic. Beyond fracture, the detail involved non-conservative modes of energy dissipation through the plastic deformation of mesh wire and frictional forces. The consideration of energy dissipation through secondary effects is not warranted for these structures.

The work summation for sufficiently small increments of displacement can be taken as:

$$U_{int} = U_{ext} \approx \sum_{\delta} \frac{1}{2} [P_{\delta_i} + P_{\delta_{i+1}}] \cdot [\delta_{i+1} - \delta_i] \quad (3.9)$$

Referring to Fig 3.3 b, the summation through each stage of loading I to IV is:

loading stage	I	II	III	IV	total
work done	277 kN-mm	307 kN-mm	1006 kN-mm	120 kN-mm	1710 kN-mm
proportion	16%	18%	59%	7%	100%

3.6.3 Composite Topping Bond

Perhaps the most notable aspect in this test was the complete and sudden loss of bond between the precast unit and the topping. The mechanics behind this bond failure are not difficult or surprising when we consider the chain of reaction to the horizontal load resulting from fracture. As discussed in section 3.5 (I), the axial force carried by the concrete section at the support prior fracture was 253 kN, which was 72% of the total axial load. Upon fracture of the Hollow Core section, most of this force was transferred to the topping slab in an instant, and was resisted by the starter bars and mesh. Over the length of the starter bars, the topping slab showed new cracks after the Hollow Core unit had fractured, but it effectively remained intact.

At a point 50mm beyond starter bar curtailment the critical crack formed across the topping slab. This crack was at least 0.6mm wide, and showed a complete fracture through the slab.

If we equate the work balance of the system, conservation of energy requires that the elastic strain energy stored in the pre-fracture floor slab must equal the total energy change in the post-fracture system. The internal strain energy of the gross pre-fracture section may be calculated and compared to the measured external work based on peak load and displacement. This involves a summation of the strain energy stored in the primary resisting elements (ie. the Hollow Core unit plus topping, starter bars and mesh wires). Because the stress distribution functions for the starter bars and mesh can be approximated as functions of length (as per eqns. 3.2), the pre-fracture strain energy can be determined:

$$U_{int} = U_{ext} \quad (3.10)$$

Written in terms of the three primary reserves of internal strain energy, and the corresponding sum of the total external work done less work due to inelastic displacement:

$$\frac{P_{max}^2 L}{2A_g' E_c} + \frac{A_s}{2E_s l_d} \int f_s^2 dx + \frac{A_{sm}}{2E_{sm} l_d} \int f_{sm}^2 dx = \sum_{\delta=0}^{\delta_{cr}} \frac{1}{2} [P_{\delta_i} + P_{\delta_{i+1}}] \cdot [\delta_{i+1} - \delta_i] - U_{\delta_p} \quad (3.11)$$

Immediately before fracture, the stress functions for the internal starter and mesh elements were:

$$\begin{aligned} f_s &= 0.66x - 135 & 200 < l_d \leq 400\text{mm} \\ f_s &= 0.0011x^2 - 0.72x + 132 & 0 < l_d \leq 400\text{mm} \\ f_{sm} &= 1.4x + 6 & 0 < l_d \leq 150\text{mm} \\ f_{sm} &= 1.2x + 40 & 0 < l_d \leq 150\text{mm} \end{aligned}$$

The elastic displacement corresponding with the maximum horizontal force is less than the total displacement at fracture because a degree of inelastic movement occurred through crack opening and slippage. This is allowed for by the subtractive term on the external work side of eqn. 3.11. Referring to Fig 3.4 b, the total stiffness of the floor system starts to reduce at a displacement of 0.14mm. This value also coincides with the level of displacement where, immediately after the topping cracked, the only increase in horizontal force is attributed to the starters and mesh. Hence, the estimated inelastic displacement is $0.27 - 0.14 = 0.13\text{mm}$. The force associated with the inelastic displacement is the average static force carried by the concrete only throughout this distance, equalling 250 kN.

For eqn. 3.11, evaluation of the internal strain energy terms becomes:

$$\frac{1}{2} \left(\frac{(352e^3)^2 \cdot 3120}{180e^3 \cdot 32e^3} + \frac{4 \cdot 113 \cdot 2.44e^6}{204e^3} + \frac{8 \cdot 22 \cdot 5.26e^6}{195e^3} \right)$$
$$33.6 \quad + \quad 2.7 \quad + \quad 2.4 \quad = \quad 38.7 \text{ kN-mm}$$

The corresponding external work done is:

$$69e^3 - 250e^3 \cdot 0.13 = 36.5 \text{ kN-mm}$$

Hence, there is some parity between the internal elastic strain energy and the conservative part of the external work done .

It has been useful to evaluate strain energy as a tool for quantifying the situation. At the point of fracture, the strain energy stored in the Hollow Core section alone was 22 kN-mm, which was 60% of total. At fracture, this energy was released almost instantaneously, and the nature of this release meant that the stiff bond surface at the interface of the Hollow Core unit and topping would have to develop a very large peak elastic shear stress if the system was not to go plastic. Because of the smooth surface between the precast unit and topping, it is almost impossible to develop the required strain energy in shear, due to the absence of a deformable volume. The problem practically becomes one of chemical adhesion, which in the case of plain reinforcing bars, for example, will generally exhibit slip at low levels of bond stress, and is certainly unreliable under dynamic loading. It is likely that the same would apply to concrete interfaces.

Because the interface could not develop the necessary peak bond stress, the released energy was transferred primarily into rupture of the topping, displacement of the floor system, plastic deformation of the topping mesh at the critical crack and increased starter bar and mesh elastic strain energy elsewhere. The hydraulic rams would have also had some role to play in energy dissipation.

3.7 Conclusions from Test A

The results of test A indicate that this detail is not suited to situations which may cause horizontal movements away from the support. This is because there is no reliable ductile mechanism available to absorb dynamic effects caused by a sudden tension failure of the stiff precast element. The internal work done did not compare well with details reported by Mejia and Park [6] for loss of support through horizontal movements. Connection Type 1 (Fig 6.4, [6]), developed 9760 kN-mm of strain energy at 55mm displacement through the inclusion of specifically designed R16 tie bars. The R16 ties had not fractured at this displacement, and therefore, a greater level of strain energy would have been achieved at failure. The quantity of work done by the standard New Zealand support region detail at failure was only 18% of Connection Type 1 at 55mm displacement.

An important aspect of the test is that the Hollow Core unit fractured through practically the entire section at the support line. Also evident was the effects of the insitu concrete binding with the void indentations caused by the plastic dams at the end of the unit. This binding contributed to the fracture by promoting a much greater tension force across the support face than would have been available with a more flush surface. It appears that the effect of edge restraint was a major factor in the failure of this detail. The combination of shear stress and axial stress was the major cause of problems for this detail through principal tension in the precast element.

The position of the fracture plane along the face of the support reduced the reliable displacement capacity, and the unit was supported on two stubs of prestressing strand no longer than 60mm long at an early stage. As the dowel action from the flexible strand waned, the unit soffit slipped below the level of the support. Three residual pieces of mesh wire embedded across the critical crack tended to peel the topping further from the unit as the precast unit progressed downward.

The topping mesh proved to have reliable strength and development characteristics, but as a cold worked steel its ductility is somewhat reduced. The work capacity of this detail was limited by the low ductility of the mesh wire.

3.8 Recommendations from Test A

Due to the poor performance of this detail under the specified loading, it is important that some consideration is given to the development of alternatives that afford ductile capacity and maintain cost effectiveness. Concurrently, there is a need to identify more closely the

structural configurations that warrant the most attention. In real structures, critical regions are likely to be where precast units have been detailed to check around columns, walls or any other stiff elements that provide edge restraint. Furthermore, these elements may be adjacent to plastic hinge zones which can undergo dilation, causing frame elongation. This would suggest that attention may need to be given to the detailing of floor layouts, with emphasis on avoiding excessively large check-outs adjacent to stiff elements and the inclusion of special steel details in these regions extending into the unit beyond the support element. The other important region would be adjacent to floor openings, where fracture line propagation may occur. Units adjacent to floor openings may also be susceptible to additional stresses, and have less redundant support reactions to rely on. These details should all be consistent with those that have been tested for performance [6,7], and attention should be given to the requirement that tie bar embedment length at least matches the strand transfer length.

Because of the very small displacement involved with fracture in Test A, it is not straight forward in recommending that special consideration should be given to one class of structure and not the other. In the case of dilation effects, it is obvious that ductile moment resisting frames are of concern, because these structures have the potential to cause fracture at the support line and pull the precast unit off the support. Alternatively, in a structure of limited ductility, sufficient force may be developed to cause fracture along the support line, but the corresponding maximum displacements are not very large. What needs to be considered is the nature of the fracture. If part of the floor fractures as in this test, it will essentially be supported at one end by a quasi form of shear friction by the strand stubs, and kinking of the mesh wire. The degree of crack opening through the topping was sufficient to reduce aggregate interlock. Hence, the resulting floor structure could not be classified as being either ductile or elastic in its design and therefore steps need to be taken to ensure that it is at least one or the other at any stage.

The geometry of the plastic void dams should be revisited. Presently these dams create a 50mm deep pocket that, once filled with insitu concrete, create significant additional brittle restraint up to the line of the support. The restraint force provided in this manner is not beneficial because dilation effects will eventually cause fracture, and this only leads to greater energy release. A shallower dam would reduce this effect and still provide a beneficial feature of a shear key acting along the support.

The use of ductile reinforcing for temperature and shrinkage steel could be considered for some structures, as this would much improve the performance of the ties across topping cracks at displacements exceeding 5mm. Topping steel, however, cannot be relied upon to uphold the floor should the precast unit slip from the support. It would also be advisable to limit the diameter of the bars used in this role to preferably 10mm and no greater than 12mm over

units where topping ties cannot be incorporated or full amplitude surface roughening cannot be achieved.

3.9 Recommendations for Future Research

It is important to note that the foregoing conclusions are based on the results of one test. It is necessary that at least a further two tests are conducted to establish some statistics. A suggestion is that one test should involve having a checkout cut in the end of the unit to simulate seating around a column, and thus verify the effects of side restraint and the point from which special tie details should extend.

A useful addition to the existing data on special support tie details would be to examine the ability of selected details to develop moment continuity and diaphragm shear. This would promote the economics of incorporating these details in buildings and would also enhance the versatility of the concept.

Chapter 4. Loss of Support: Test B

4.1 Description of Support Detail

This test examined a support detail that has been developed by Firth Stresscrete for short seating or nil seating applications (Figs 4.1).

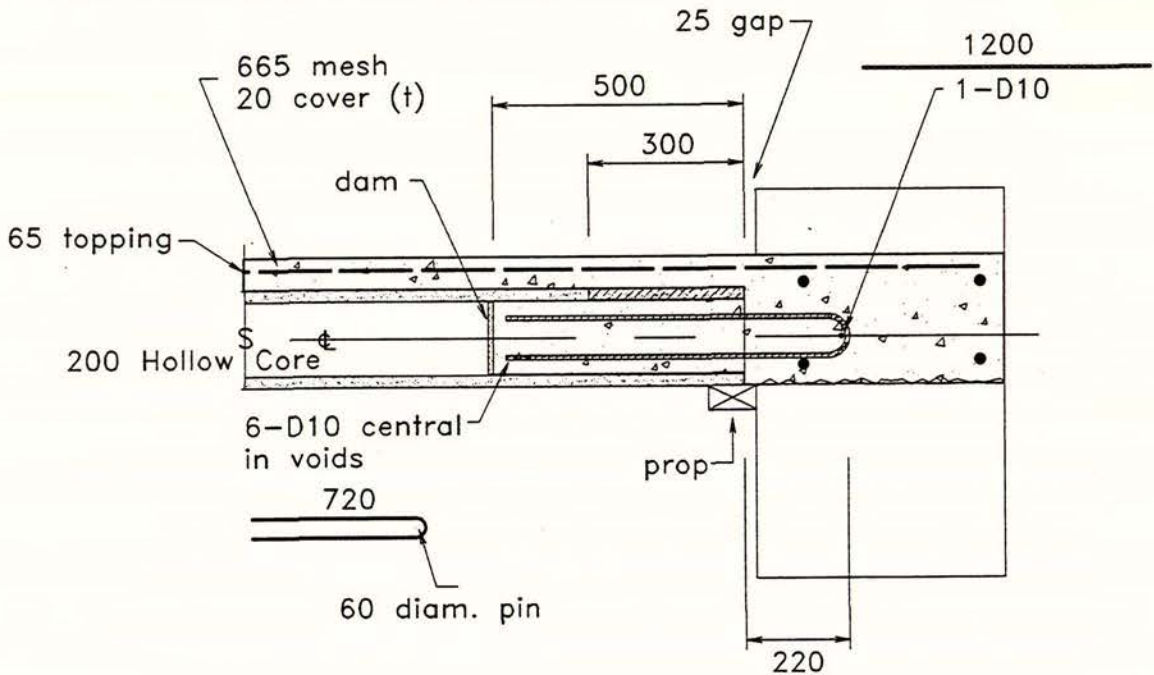


Fig 4.1 a: Firth Stresscrete nil seating detail for 200mm Hollow Core



Fig 4.1 b: Example of the nil seating detail

This detail has been designed to utilise the principals of shear friction for transferring gravity loads to the supports. This is achieved by placing 10mm deformed bar hairpins in each of the "broken back" Hollow Core voids and securing them with insitu topping concrete. In accordance with eqn 7-23 of the New Zealand concrete design code [1], the reliable ultimate shear capacity of this detail, developed through shear friction is:

$$V_u = (A_{vf} f_y - P_u) \phi \mu \quad (4.1)$$

$$\therefore V_u = (12 \cdot 79 \cdot 300) 0.75 \cdot 1.4 = 300 \text{ kN}$$

Eqn. 4.1 demonstrates that provided no significant axial tension exists in the section, this detail is capable of sustaining shear forces well in excess of those that would normally be allocated to a 200mm Hollow Core unit. In the case of frame dilation, axial displacements imposed by the frame members are sufficient to exceed the yield strain of the hairpin bars, thus introducing a tension force equal to P_u in eqn. 4.1. At this point, shear friction as such is reduced to zero, however, providing that the crack opening is still small, reliable shear strength can still be maintained through aggregate interlock and bar dowel action [10]. The contribution of aggregate interlock is no longer considered effective at displacements exceeding 1.0mm [3]. Because of the large displacements involved with frame dilation and the size of reinforcing used, only bar kinking needs to be considered for this detail.

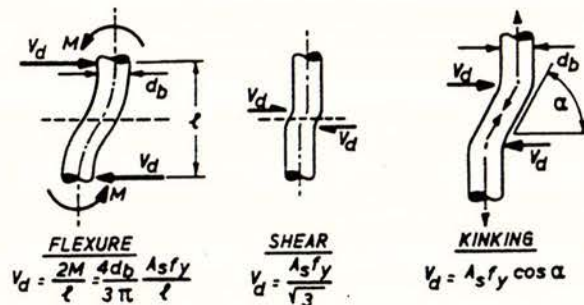


Fig 4.2: Mechanisms of dowel action across a shear interface

4.2 The Detail Tested

Test B was constructed as follows:

precast unit	topping	G300 hairpins	bar embedment	mesh
200mm H. Core	65mm	6 No. D10	500mm into unit	665 (5.3mm)

For this test, the 665 mesh was carried over into the support member.

4.3 Materials

4.3.1 Concrete

For the topping concrete, a design strength of 35 MPa was used in order to achieve an insitu crushing strength greater than 25 MPa in a comparatively short period. Although it is possible to achieve the design strength in seven days with continual wet curing, this duration is unrealistic for most practical applications. Ideal moist curing is lacking on most building sites, therefore, it was opted to order a higher grade of concrete and allow only three days of curing using damp hessian cloth. The ordered concrete mix:

design strength	max. aggregate	ordered slump
35 MPa @ 28 days	13mm	100mm

The topping for this test was received at a slump that was well within tolerance for a snatch sample, and could be described as a good, workable mix. The topping concrete properties were as follows:

slump received	test insitu strength
85mm	31 MPa @ 11 days

4.3.2 Reinforcing Steel

Tensile tests were performed on the 10mm diameter grade 300 bars and the 665 wire mesh. Measurements were also made of the total elongation of each test specimen at fracture:

taken over three specimens:	avg. yield stress	avg. UTS	avg. ϵ_{sh}	avg. strain at UTS	avg. strain at fracture
D10 bar	312 MPa	434 MPa	2.53%	16.3%	23.6%

avg. E = 205 GPa

taken over three specimens:	avg. proportional limit	avg. UTS	avg. strain at fracture
665 mesh	528 MPa	660 MPa	5.4%

avg. E = 196 GPa

For the hard drawn wire specimens, the maximum and minimum elongation's measured at fracture were 6.4% and 4.1% respectively.

4.4 Results of Test

The behaviour of test B is illustrated in Figs. 4.3.

The initial response to loading produced little displacement. The first cracks had appeared along the line of infill concrete at a load of 250 kN, and were approximately 0.1mm wide. At a load of 441 kN, a small plateau occurred, with an increment in displacement from 0.85mm to 1.4mm. From this point, the contribution of concrete tension was lost, and the stiffness reduced markedly. The horizontal force increased at a steady rate up to the peak load of 520 kN at 7.2mm displacement.

Beyond the peak horizontal load, the mesh wires began to serially fracture, and this was continued out to a displacement of approximately 21mm. From 25mm displacement a plateau occurred at which the D10 hairpins approached fracture elongation, and failure of the hairpins began at 38mm. From 38mm to 43mm the load response decreased rapidly as seven of the twelve hairpin legs fractured. A second smaller plateau occurred out to 49mm when a further three legs fractured. The third plateau occurred from 50mm out to the terminal displacement of 55mm. The specimen was supported on two legs of reinforcing throughout this phase of the test. At this point the unit had dropped below the support, kinking the remaining bars downward by a average of 8mm. The specimen finally failed under the additional weight of the technician who had climbed onboard to place the vertical ram load cell. Paul Murphy doesn't weigh much, and he was even lighter after this experience.

The progress of this test was steady, showing few surprises other than the exceptional ending.

4.5 Analysis of Test Results

Fig. 4.3 b shows the load-displacement diagram divided into five regions of significance. These regions characterise the load response to horizontal displacement, with each illustrating a change in the basic mechanism of load resistance.

Load-Displacement (Test B)

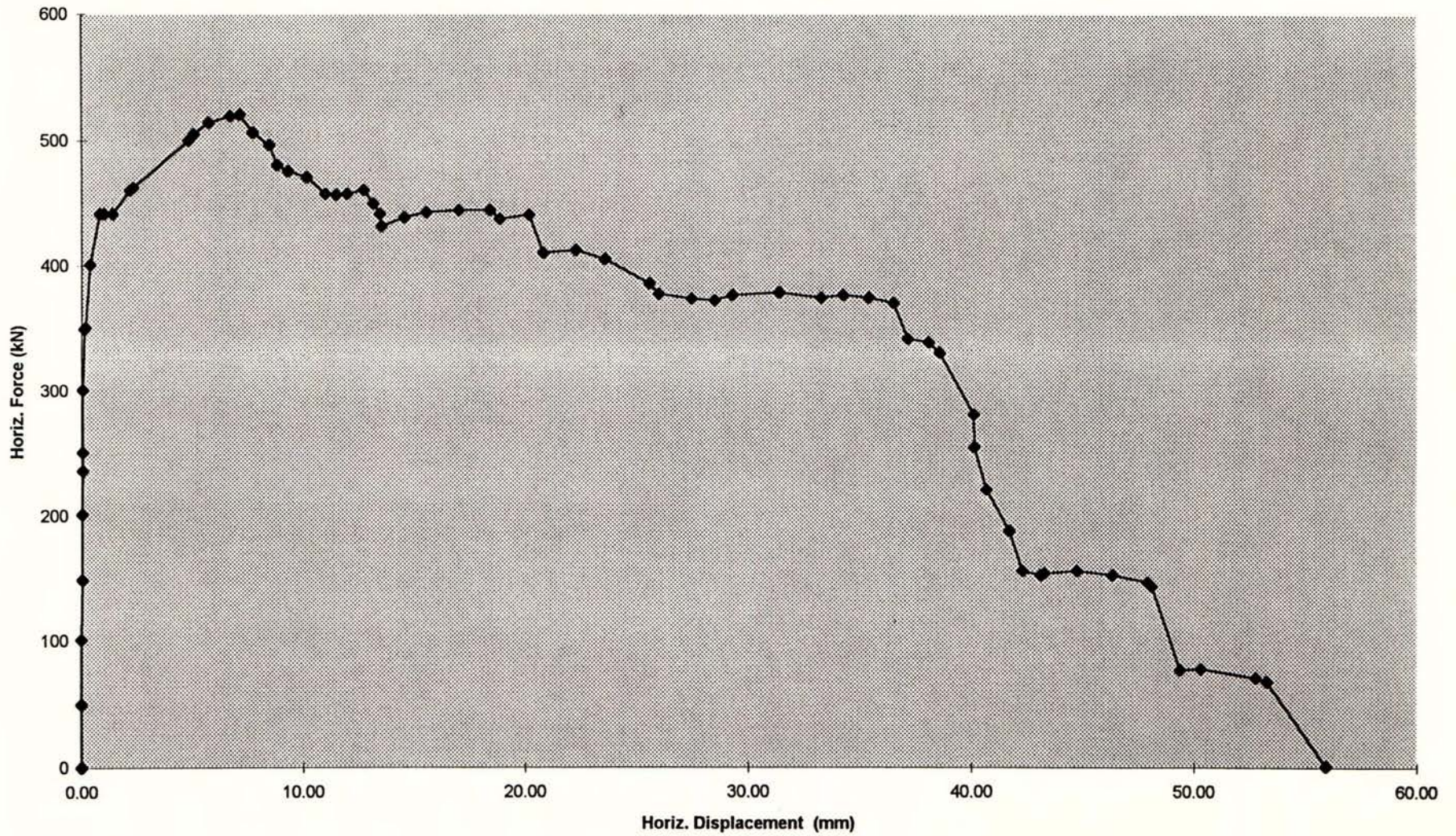


Fig 4.3 a: Load-Displacement diagram for test B

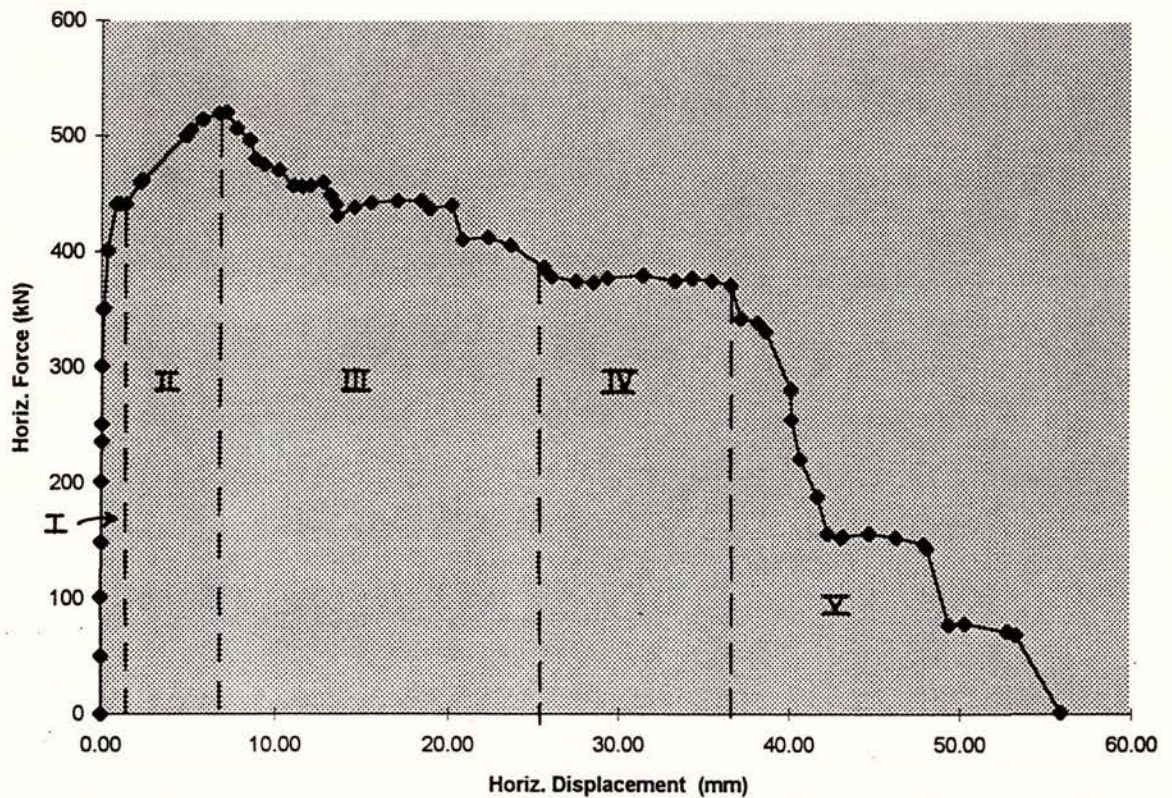


Fig 4.3 b: Load-Displacement diagram divided into regions of significance

(I) Loss of Concrete Tension

From zero to 0.4mm displacement, the section exhibited elastic properties with a stiffness of 1025 kN/mm. Immediately beyond 0.4mm, the section had softened rapidly at a second stiffness of 90 kN/mm, out to the point where the section effectively became inelastic at 0.85mm. During this phase of the test, the concrete ruptured along the 25mm wide insitu strip between the end of the unit and the support beam.

At 0.14mm displacement, the wire mesh had begun to register stress, and had achieved 150 MPa at 0.2mm, increasing to 400 MPa at 0.4mm. The D10 hairpins began to register stress at approximately the same time as the mesh, and had typically achieved yield stress by 0.4mm displacement. The proportion of force carried by the concrete is shown in Fig. 4.4 as the difference between the total force and the steel force. The steel force is calculated from the average of four gauge stations in the 25mm insitu infill strip between the Hollow Core unit and the support block. Fig. 4.4 indicates that the concrete lost practically all of its tensile capacity by 0.2mm displacement, but continued to have a small residual strength up to 0.8mm. The section as a whole behaved elastically up to 0.4mm displacement, and this would have been due to the D10 hairpins reaching yield strength.

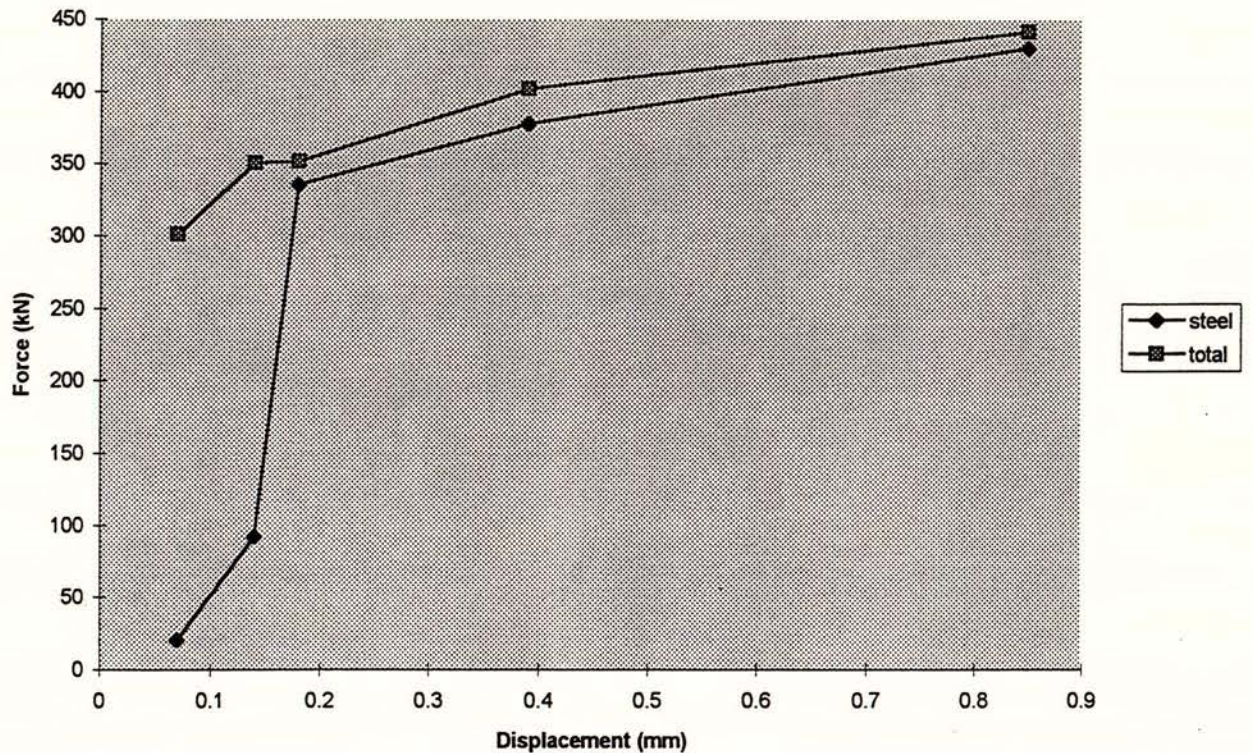


Fig 4.4: Proportion of forces in section at stage I

(II) Post-Cracking to Peak Load

From 0.85mm displacement to peak load at 7.2mm displacement, the wire mesh made a short but significant contribution to the reaction force. At the end of this stage, the mesh carried 22% of the total load of 520 kN. The D10 hairpins had all reached strain hardening by 2mm displacement, and at the end of stage II, they had obtained an average of elongation of 5.9% at the critical section.

During this stage, a crack that had begun to initiate late in stage I became more pronounced. The crack was situated in the Hollow Core unit (Fig. 4.5) and in the early stages of the test it opened at approximately the same rate as the principal crack across the support. During stage II of the test, this crack reached a maximum of about 5mm at the top of the unit and 3mm at the soffit, and hence, formed an average crack width of 4mm through effectively one half of the Hollow Core unit. Referring to Fig. 4.5, it is evident that the placement of the prestressing strand has some effect on the formation of cracks. In this unit, no strands were located at the edges of the unit. The effect of this can be traced by the shape of the crack in the slab. The crack starts at 165mm from the end of the unit at the side, and extends towards approximately the centre of two the unit at an angle of 16° . The course of the crack is visibly effected by the presence of two strands, the first at 220mm from the side of the unit. At this

point, the strand would have probably developed 20% of its maximum force in the concrete. Because this crack is caused by tension normal to the line of the crack and not by shear, the component of strand compression will cause a change in the orientation of the crack line by introducing shear stress above that which may already exist through aggregate interlock along the crack.

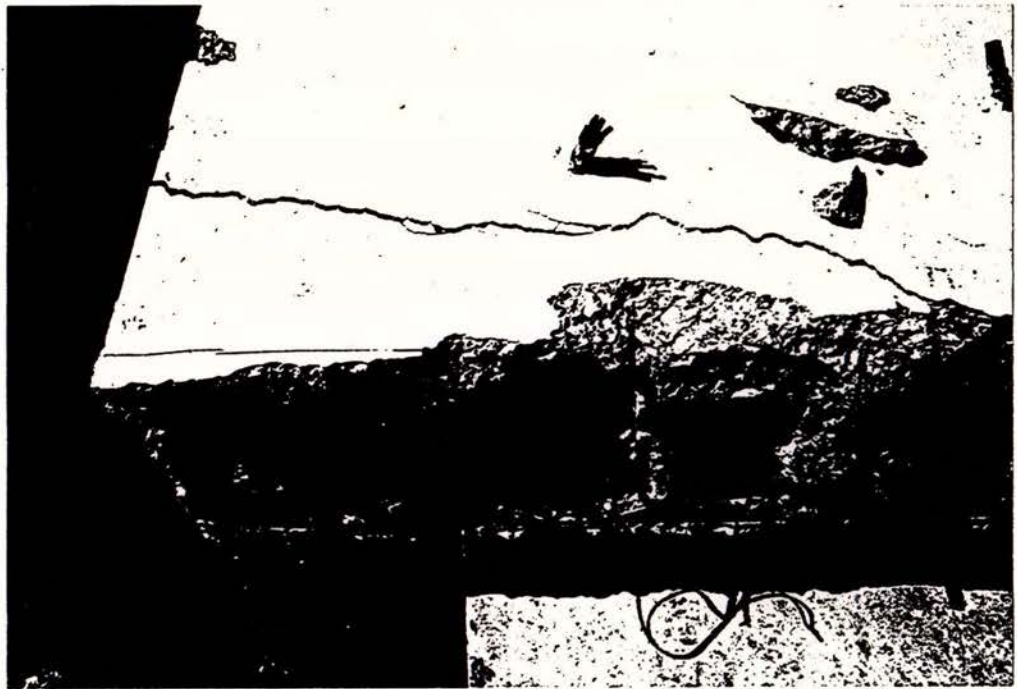


Fig 4.5: View of Hollow Core slab showing crack through section

(III) Peak Load to Loss of Mesh

From peak load displacement at 7.2mm through to 22mm displacement, the reaction force dropped in two notable steps from 520 kN to 412 kN through fracture of the topping mesh. From 22mm to 26mm the reaction gradually dropped to 375 kN as the extension of the D10 hairpins moved past the peak stress plateau of the stress-strain relationship. The peak stress elongation had been reached during this stage of the test at approximately 15mm displacement. Figs. 4.6 show the respective stress distributions along the mesh wire and D10 hairpins. At 20mm displacement, the effects of bar slippage and strain penetration are indicated by the upper line on Fig 4.6 b.

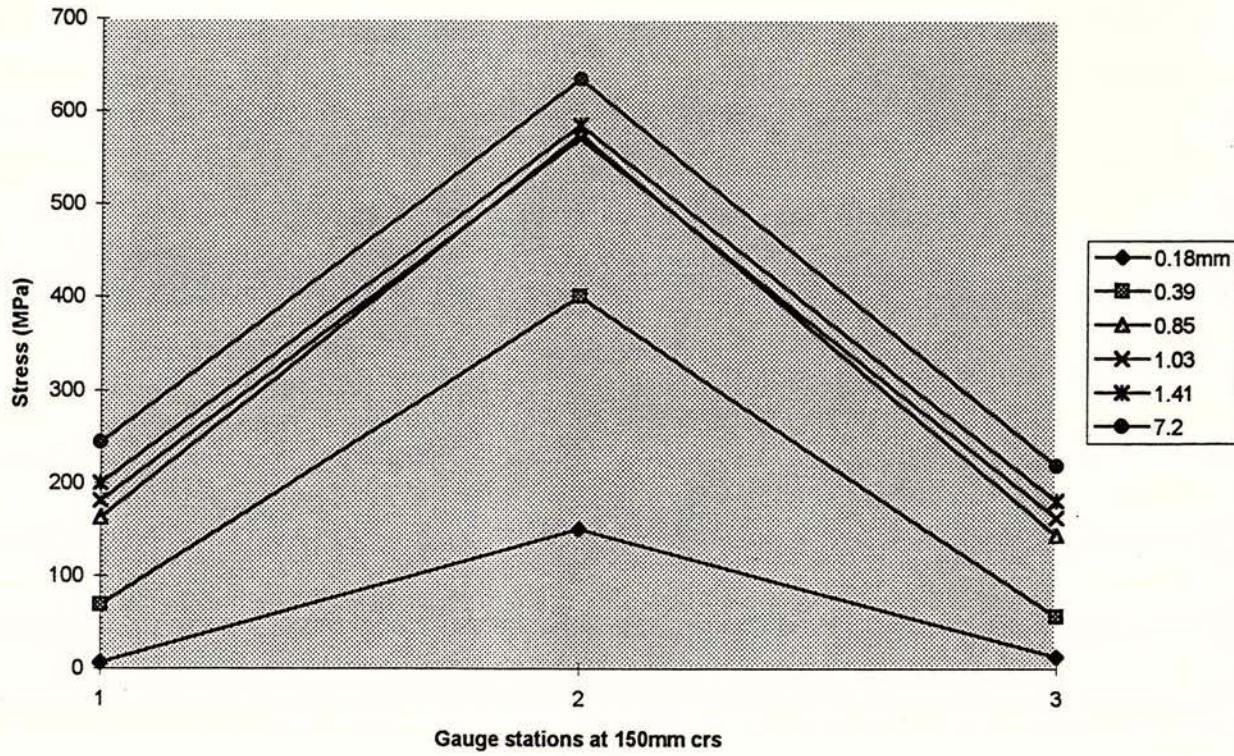


Fig 4.6 a: Stress distribution along 665 mesh at the onset of fracture

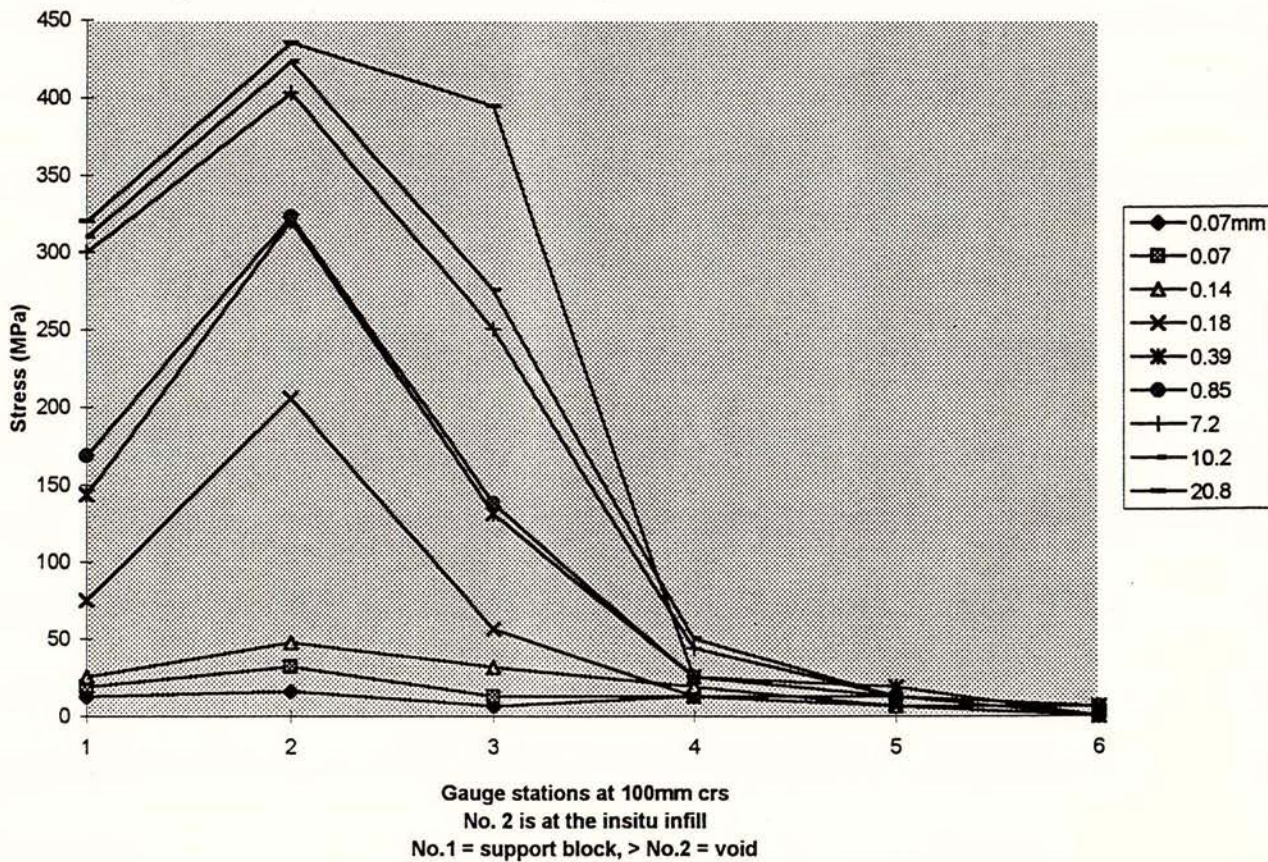


Fig 4.6 b: Stress distribution along D10 hairpins up to end of stage III

(IV) Plateau Region to onset of Hairpin Fracture

This region shows a plateau in the reaction from 26mm to 37mm displacement. This was probably caused by a combination of three components. At this extension, some of the hairpins would be approaching fracture and some would still be at an extension corresponding to peak stress. Also at this point there would be a significant amount of slippage and strain penetration into the section adjacent to the critical crack. The net effect is that an equilibrium state is caused by the declining force in the bars approaching fracture being balanced by the bars near peak stress being afforded extra gauge length. Examination of the test specimen clearly indicated that physical penetration into the adjacent concrete did occur, with cleanly fractured cones of 10 to 15mm around most bars.

(V) Hairpin Fracture and End of Test

From 37mm extension the hairpins failed rapidly, with seven of the twelve legs failing in the first volley. This occurred in a space of 5mm, in which the reaction dropped from 375 kN to 155 kN. From 42mm to 48mm a second plateau occurred until a further three legs failed, reducing the reaction to 77 kN. The final small plateau went from 48mm to 55mm on the remaining two legs of D10, where the reaction was dropped to 68 kN, and failure was imminent. Then detail had survived just to the end of the 55mm design displacement, and failed under the additional weight of the technician.

Immediately before failure, the end of the unit had sagged an average of 8mm below the support line, and was clearly seen to be supported on the two remaining bars. The bars were both at the top, one at the edge and the other at the centre. The total free length of bar (ie. including penetration) was measured over several samples and was found to be a good average of 84mm. This figure is 53% above the design displacement of 55mm and represents a combination of bar elongation and slippage.

4.6 General Analysis

4.6.1 Ductility and Work Done

Although this detail generally "behaved" and exhibited an excellent peak load capacity, it is obvious that the ductility was not adequate for situations where severe frame dilation could occur. This was essentially due to the extremely efficient bond that exists between well compacted confined concrete and small diameter deformed bars. Referring to Fig 4.6 b, it is evident that the bar can develop its overstrength capacity in an embedment length of less than 200mm of straight bar. At the hook end, strength would have probably developed in less than

this distance, and so most of the strength development and certainly the slippage would have occurred in the 100mm between the critical crack and the hook tangent. Even though the gauge length of the hairpins was changing continuously due to strain penetration and slippage, if we take the point on either side of gauge No.2 (Fig 4.6 b) where bar yield has been reached, and use this as an estimate of the bar gauge length, the maximum available crack opening is:

$$\Delta L = \epsilon_u L_0 \quad (4.2)$$

$$\therefore \Delta L = 0.24 \cdot (100 + 120) = 53 \text{ mm}$$

The work done by this detail was impressive, developing a total of 18,700 kN-mm of strain energy through 55mm of horizontal displacement.

4.6.2 Dowel Action at the Support

The support reaction across the tested detail was calculated to be 12.2 kN. At the end of test, the measured bar angle was approx 8° to the line of the unit, and the estimated bar stress over the two remaining bars was 400 MPa on the original section. From eqn. 4.3, the support reaction provided through dowel action of the hairpin bars can be calculated for any stage of loading if the angle α is known.

$$V_d = A_s f_y \sin \alpha \quad (4.3)$$

Therefore at the end of test:

$$\therefore V_d = 2 \cdot 79 \cdot 400 \cdot \sin 8^\circ = 8.8 \text{ kN}$$

Though this is somewhat lower than the actual reaction, the unit was partially supported on the projecting legs of fractured hairpins. This is because as the unit rotated, it pushed into and was "spiked" by these residual pieces of bar.

The angle α is not easily estimated as an exact value for an application, because it will vary according to the geometry of the floor, the magnitude of crack opening and the floor gravity and seismic loading. As a capacity design approach though, this angle may be prescribed to a safe upper limit, and a value of 30° has been suggested based on punching shear applications [3]. The capacity of the detail based on this angle would be:

$$V_d = 12 \cdot 79 \cdot 300 \cdot \sin 30^\circ = 142 \text{ kN}$$

4.7 Conclusions from Test B

It appears that the detail tested has good potential as a method of supporting Hollow Core units in situations of short seating and *small* horizontal movements through dilation of the floor. The peak load performance was excellent, with bar anchorage being maintained at all stages of the test. The major drawback was ductility performance, which becomes a priority for details subject to the severe dilatational type displacements associated with seismic load resisting frames. It is envisaged that the detail would perform less well than it did for this test due to larger end reactions and load cycling in a real structure. In this test, the 55mm achieved is slightly artificial, and the true reliable displacement is more likely to be a maximum of 30mm considering the variability in loading already mentioned.

It would appear that for smaller displacements (eg. 30mm) the shear capacity developed by dowel action is adequate for the levels of load normally supported by these floor systems. This is provided that the Hollow Core unit does not peel along the webs. This effect was not able to be examined in this test due to the large load that would be required. Because the specimen did not survive the prescribed displacement of 55mm, significant vertical load could not be applied. Peeling of the Hollow Core unit was observed in the tests done by Mejia [6] and was caused by the straightening of two 16mm diameter tie bars that were embedded in cores. In the case of straight D10 hairpins the mechanics of the situation are related, but some basic differences do exist.

The occurrence of a large crack through the Hollow Core unit and topping (Fig 4.5) highlighted the important role of strand forces on the control of tensile cracking in this form of construction. Because no reinforcing exists to control cracks, other than the prestress force and bond of the longitudinal strands, regions immediately adjacent to the support may be subject to fracture. This emphasises the fact that all tie bar details must be embedded to at least the transfer length of the prestressing strands if the full capacity is expected to be developed.

4.8 Recommendations from Test B

The essential recommendation for this test is that the detail is changed to develop greater ductility than was demonstrated. This can be achieved, based on existing knowledge, by replacing the D10 hairpins with R10 paperclips (Fig. 4.7). Plain bars, by allowing slip to occur between the bar surface and the surrounding concrete, create a longer gauge length for the ultimate strain capacity to act upon, thus increasing the elongation at fracture. The bond stress for plain bars is usually assumed to be one half that for deformed bars, thus development length in general terms is taken to be twice as long [1]. Tests on details incorporating plain bars have

indicated satisfactory performance in this role [6], and plain bars are recommended by the FIP [7] for use in situations where large elongation is foreseen. An additional alteration to the existing detail is to allow a greater length of bar between the tangent of the hook and the location of the critical crack to allow slippage over this portion of the tie. It is suggested that the minimum distance from the edge of the support to the end of the tie is 200mm. On well confined support details, this also removes the need for a D10 anchor bar in the hook as was originally detailed. For a plain bar detail hook returns are required at both ends, hence, the term "paper clip".

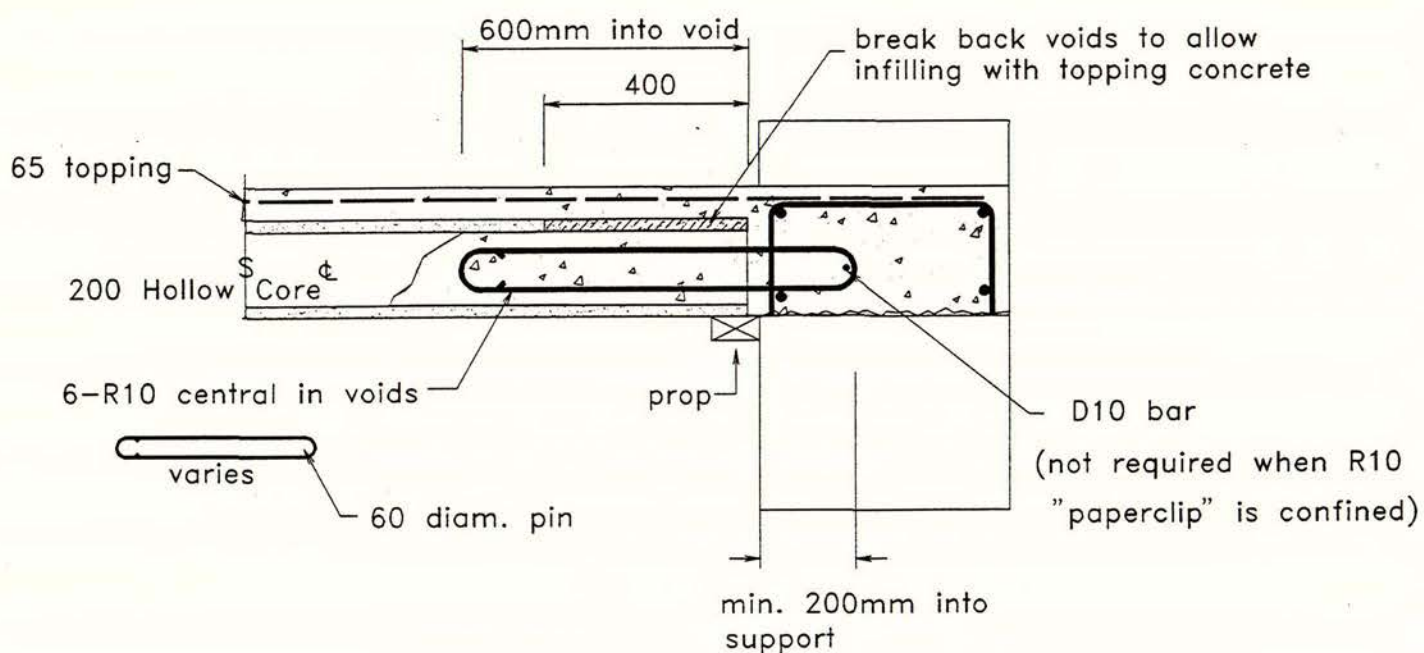


Fig 4.7: Recommended detail for nil seating and loss of support

4.9 Recommendations for Future Research

Probably the most useful research would be to determine the dowel action capacity of the paperclip detail in shear after dilatational loading, especially with regards to possible peeling of the Hollow Core section through the webs.

Chapter 5. Translation and Diaphragm Action

5.1 General

The aim of this testing is to introduce load configurations into the support details of Hollow Core floor units that are consistent with the diaphragm actions in a structure that may experience frame dilation. In the diaphragm action tests, emphasis is placed on examining the ability of details to sustain forces and rotations induced by diaphragm "beam" action, and translation of the supports with combined dilatational movements. These experiments compliment the Loss of Support tests because they specifically examine the ability of Hollow Core ends to sustain compressive loads caused by diaphragm action in a severe earthquake. If it is found that Hollow Core sections can fail under loads and displacements consistent with diaphragm actions, then suitable details will need to be implemented to maintain structural integrity. An equally important aspect of this testing is the composite bond performance of the topping concrete and the behaviour of continuity bars and starters under cyclic loading.

The translational displacement associated with this testing serves two purposes. When translation is applied without concurrent axial compression, a simulation is made of floor units seated in the corner regions of building frames. In these parts of a seismic load resisting frame, plastic hinge dilation is likely to cause frame expansion in both the longitudinal and transverse directions. Hence, the seatings of floor units in these regions will experience sideways movement combined with elongation resulting from the longitudinal dilation. The reaction to these displacements will be provided by the starter or continuity bars in the topping. Alternatively, when axial load is applied concurrently with translation, simulation is made of the end region of a building where significant frame dilation does not occur parallel to the floor units. This loading format also applies to the centre region of the building where translation and significant axial compression can model the combined stresses occurring at the support due to diaphragm beam action. This later simulation is best accomplished by post-tensioning the floor slab through the Hollow Core unit with a layer of prestressing strands. Illustrations of the described diaphragm actions are shown in Figs. 5.1.

The degree of dilation that can occur in the plastic hinge of an unrestrained beam is known to be in the order of 2 to 8 percent of the beam depth [3]. Depending on the structural configuration, it is likely that dilations of reasonable magnitude could occur on a localised basis, especially at the junction of beams and columns. In the case of floor units seated into these areas, restraint provided by starter bar ties along the side of the unit may be of little consequence (Fig 5.1 b).

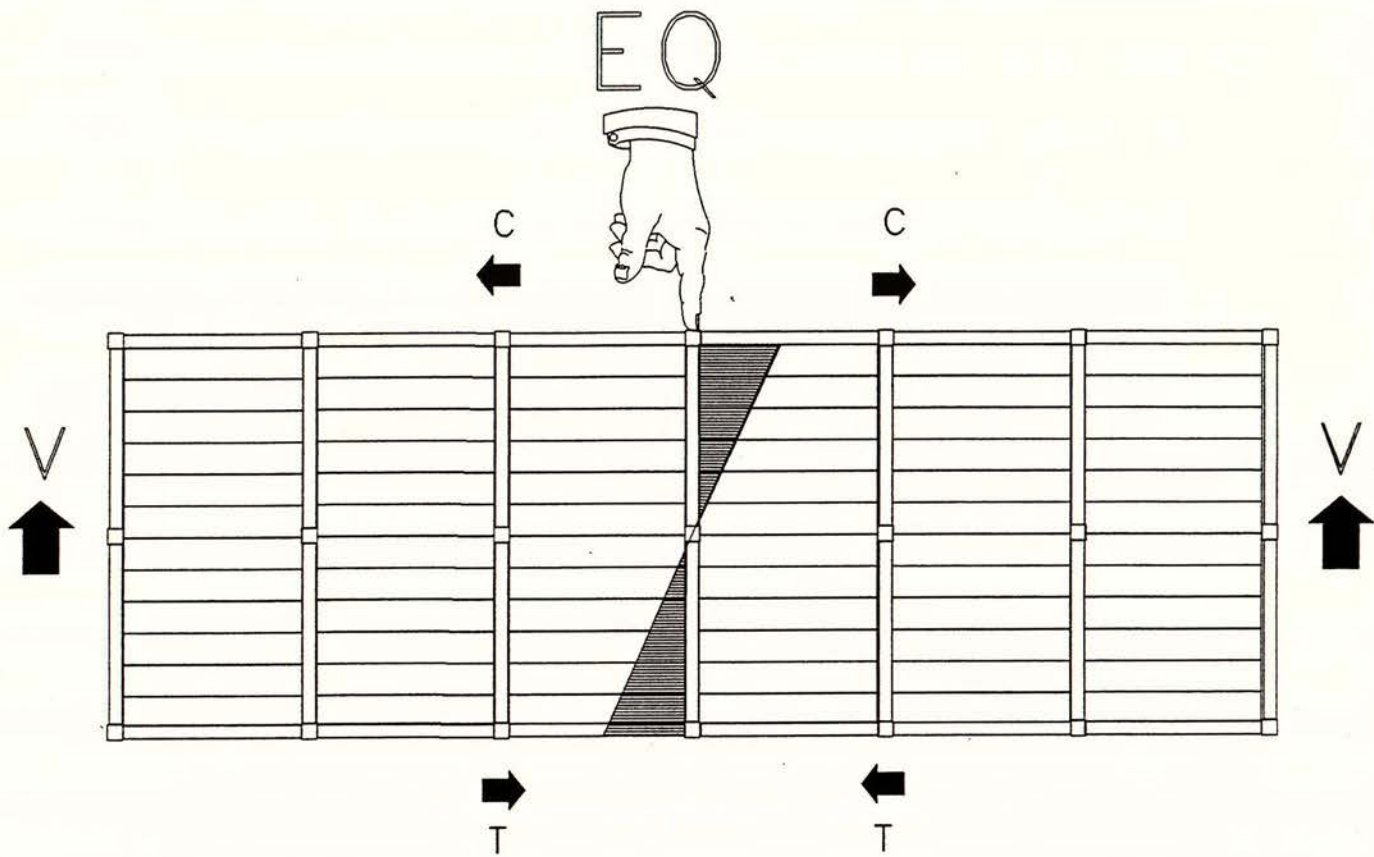


Fig. 5.1 a: Diaphragm beam action under seismic loading

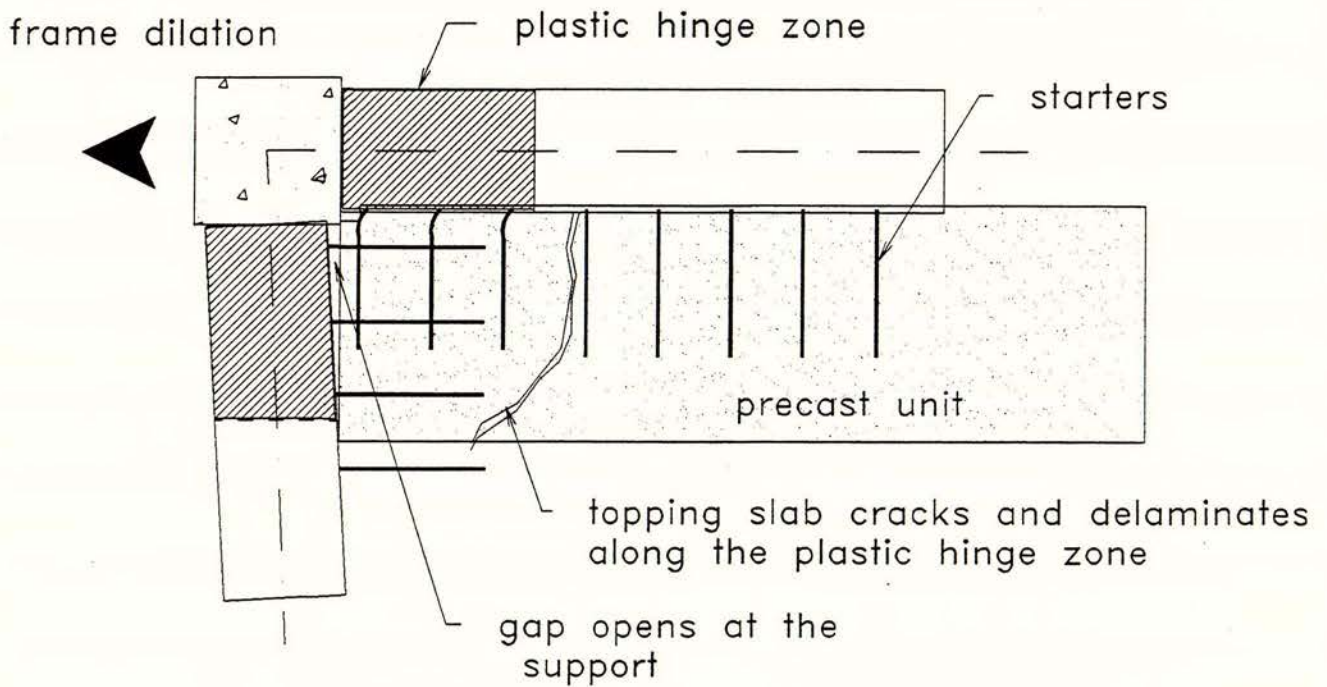


Fig. 5.1 b: The effects of frame dilation in corner regions

5.2 Description of the Test Rig

The basic layout of the test rig for combined translation and axial load is shown in Figs. 5.2. The support detail is identical to that used in the Loss of Support test A, representing the most commonly used detail in New Zealand for Hollow Core flooring. As discussed in section 3.1, this detail relies on the composite bond capacity between the precast unit and the composite topping for the transfer of diaphragm forces. It is therefore essential that adequate bond is maintained between the precast element and topping and that the integrity of the detail is not reduced by excessive spalling and loss of cover concrete. The performance of the detail can be observed for varying quantities and sizes of continuity and starter bars as they occur in real structures.

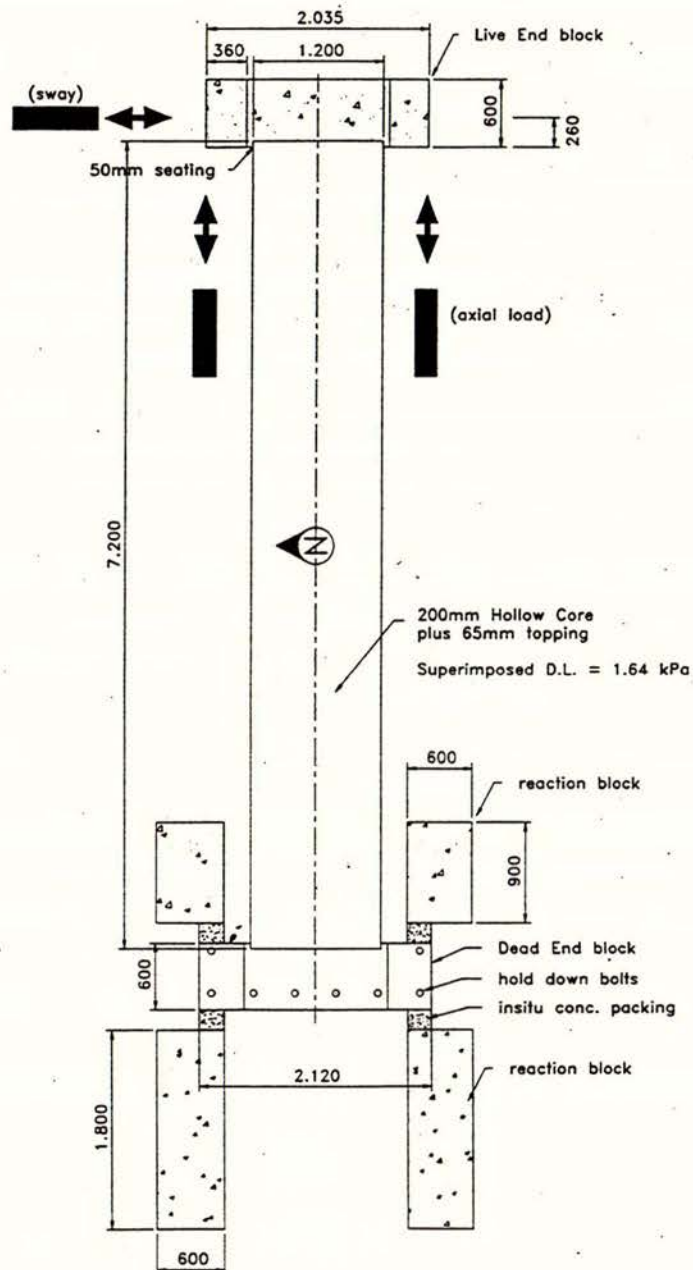


Fig 5.2 a: Plan of combined sway and axial load test rig

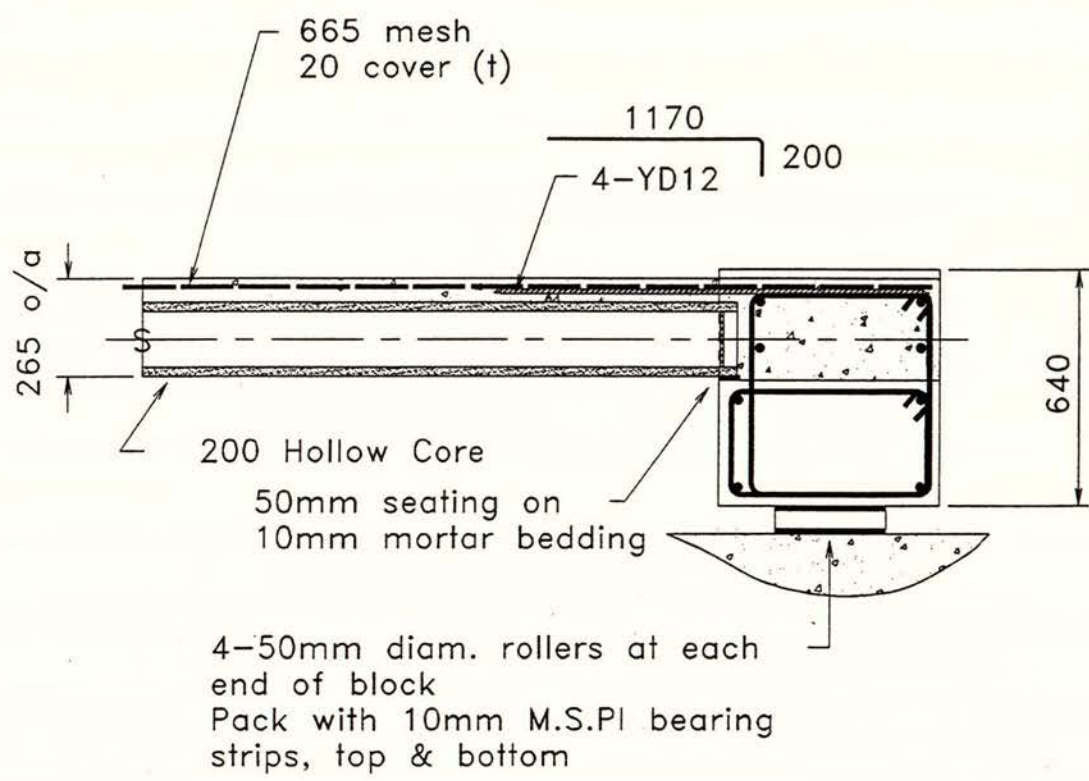


Fig 5.2 b: Elevation of sway end support

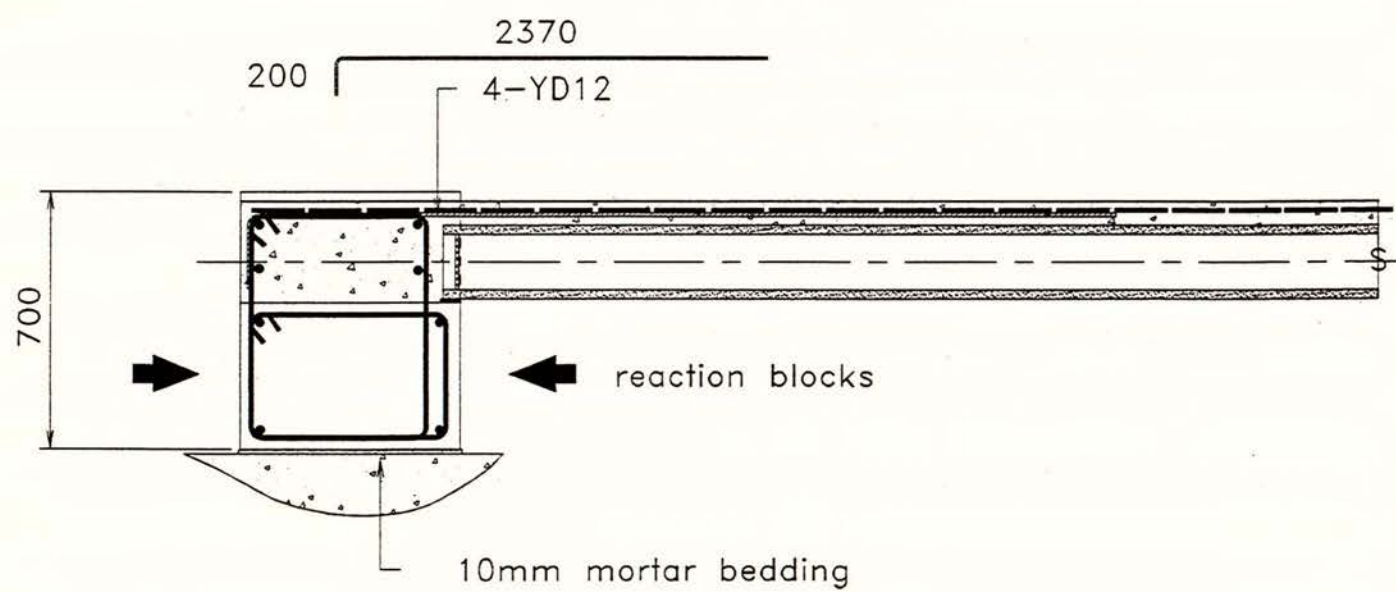


Fig 5.2 c: Elevation of fixed end support

5.2.1 Translation and Axial Load

The lateral sway in this test is provided by a single 43 ton double acting hydraulic ram. The ram is attached at what is termed the "sway" end of the test rig, and in this manner forms the loaded end of a cantilevered test setup. The support block is seated onto eight 50mm diameter by 300mm long rollers, packed between 10mm steel plates which effectively allow lateral travel with little resistance (Fig. 5.2 b).

Axial load may be applied either through two 43 ton double acting rams attached to the sides of the sway end support block, or by post-tensioning with prestressing strand through the voids of the Hollow Core unit and anchoring the strand at the support blocks (Fig 5.2 c). The application of prestress is ideal for modelling large compression forces as it requires no direct external reactions being placed on the test rig to overcome this force.

5.2.2 Vertical Loads

Throughout these tests a superimposed dead load of 1.70 kPa is provided, in addition to the floor self weight, starting at 1.2m from the support line at each end. A feature of this test setup is that the support lines show cracks prior to the application of lateral loading at the sway end. This is done to incorporate the fact that cracks form along the support lines in real floors due to flexural actions and concrete volume changes. To induce cracks in the test unit, a vertical load can be applied through the overhead ram apparatus used in the Loss of Support tests (Fig 2.3).

5.3 Instrumentation

5.3.1 Hydraulic Ram Forces

The ram forces in this test are measured in identical fashion to the Loss of Support tests, section 2.3.1.

5.3.2 External Displacements

100mm potentiometers were placed at the sway end block to measure lateral and outward displacements. Other potentiometers were placed on the test rig to measure differential displacements between the topping and the precast unit (Fig 2.4), and also shear displacement between the floor unit and the support block. Dial gauges were used to monitor slippage of the reaction blocks at the fixed end of the test rig.

5.3.3 Bar Strains

Electrical resistance strain gauges were connected to the principal reinforcing to establish bar strain characteristics. The strain gauges used in this test were all ordinary 3% gauges as described in section 2.3.3 of this report.

5.3.4 The Data Logger Unit

The load cells, potentiometers and gauges were connected to the data logger unit as described in section 2.3.4 of this report.

Chapter 6. Sway and Axial Load: Test A

6.1 Description of Support Detail

This test examined the support detail shown in Figs. 5.2 b&c with four HD12 starters and continuity bars at the sway and fixed ends respectively. The wire mesh was curtailed at the end of the Hollow Core unit and did not form part of the detail reinforcing. This configuration was chosen as a starting point for this series of tests, representing the lower bound of reinforcing steel in the support region. A light reinforcing configuration was also chosen for the purposes of constructing a specimen with similar proportions to the floor that failed in the Los Angeles earthquake of January 1994 (Fig. 1.1), with the exception of being a typical New Zealand detail.

6.2 The Detail Tested

Test A was constructed as follows:

precast unit	topping	G430 cont. / start.	bar embedment	mesh
200mm H. Core	65mm	4-HD12 @ 300 crs	1800mm / 600mm	665 (5.3mm)

6.3 Materials

6.3.1 Concrete

For the topping concrete, a design strength of 30 MPa was used in order to achieve an insitu crushing strength greater than 25 MPa in a comparatively short period. Although it is possible to achieve the design strength in seven days with continual wet curing, this duration is unrealistic for most practical applications. Ideal moist curing is lacking on most building sites, therefore, it was opted to order a higher grade of concrete and allow only three days of curing using damp hessian cloth. The ordered concrete mix:

design strength	max. aggregate	ordered slump
30 MPa @ 28 days	13mm	90mm

The concrete received was at a slump of 150mm, however, it was accepted because it showed good consistency, with no signs of bleed water when vibrated. The high slump did however reduce the 28 day strength expected for a block with seven days moist curing.

slump received	test insitu strength
150mm	25 MPa @ 28 days

6.3.2 Reinforcing Steel

Tensile tests were performed on the 12mm diameter grade 430 bars and the 665 wire mesh. Measurements were also made of the total elongation of each test specimen at fracture:

taken over three specimens:	avg. yield stress	avg. UTS	avg. ϵ_{sh}	avg. strain at UTS	avg. strain at fracture
D10 bar	446 MPa	587 MPa	1.88%	12.3%	21.6%

avg. E = 204 GPa

taken over three specimens:	avg. proportional limit	avg. UTS	avg. strain at fracture
665 mesh	528 MPa	660 MPa	5.4%

avg. E = 196 GPa

For the hard drawn wire specimens, the maximum and minimum elongation's measured at fracture were 6.4% and 4.1% respectively.

6.4 Axial Loading and Test Format

Because this test examined the performance of a floor unit in similar circumstance to that in the Los Angeles earthquake of 1994, it was chosen to use a seismic load derived from the provisions of NZS 4203: 1992 " General Structural Design and Design Loads for Buildings " [12] for a building of similar geometry and construction as a basis for comparison. The basic layout of this building (Fig 6.1) shows a twin level parking structure (ground plus roof) with a block masonry perimeter on three sides, and tied along the open side by a perimeter beam at the level of the Hollow Core roof structure. The precast floor units span 7.0m over seven bays, with overall building dimensions of 50m long by 10m wide. The interior beams are steel UB sections supported on cantilevered steel columns with flexible connections to the beam soffit.

From section 4.2.6 of [12], the seismic weight for this structure is: $G + \psi_u Q$. Allowing 4.0 kPa for dead load and 2.5 kPa for a parking structure and 0.4 for the live load combination factor ψ_u , the seismic weight for the floor is 5 kPa, and therefore 50 kN/m over the width of floor. Adding to this the half storey weight of the perimeter block wall, assumed filled, the total weight per length of building is 57 kN/m, = 2850 kN over the entire building.

From section 4.6.2.7 of [12], the seismic coefficient is: $C = C_h S_p R Z L_u$. For a block masonry structure the structural ductility factor μ is 2. Assuming a structure on intermediate soils, the resulting value of C_h is 0.49, and for a building of normal usage in a seismically active zone, the resulting coefficient is: $C = (0.49)(0.67)(1)(1)(1) = 0.33$. This value applied to the seismic weight results in a seismic shear of 940 kN. The moment due to earthquake loading is therefore equal to $\frac{Wl}{8} = 5875$ kNm, the corresponding chord force is $\frac{M}{b} = \frac{5875}{10} = 588$ kN.

At the perimeter, this force is resisted by the chord beam, and therefore it was decided to use a force of two thirds this value, representing the force at the compression centroid of the elastic diaphragm. The axial force used in test A is therefore 400 kN.

The test format chosen was to initially sway the specimen without the addition of axial load, and this was done for two reasons. The first reason was to see whether the insitu support block concrete would restrain the unit by developing tension forces at the Hollow Core void indentations. Tension developed in this manner was a major factor in the performance of the Loss of Support test A (section 3.7). The second reason was to allow the development of cracks along the support line and thus help reduce the confinement produced by clamping between the topping concrete and the support ledge. In the second phase of the test, 400 kN of axial compression was applied to the end of the sway end, and the unit was then displaced in a cyclic pattern.

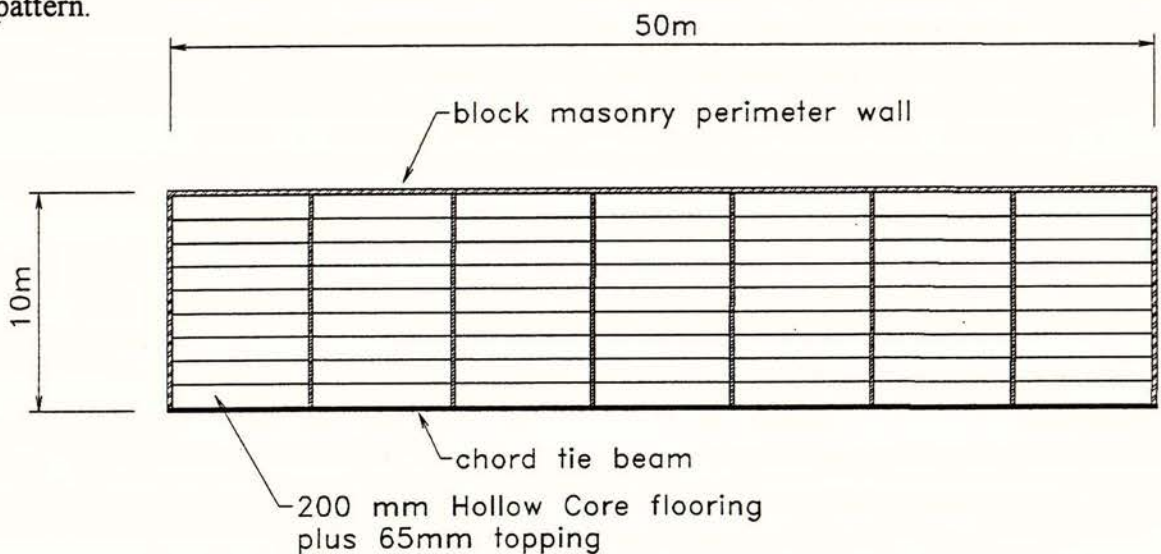


Fig 6.1: Plan of example structure

6.5 Results of Initial Loading

The load-displacement curve from the initial loading phase of this test (Fig 6.2) indicates that no significant restraint was present due to concrete binding at the void indentations. The curve indicates a ductile response, with yield occurring at about 8mm displacement with a corresponding lateral load of 14 kN. At six times yield displacement, the lateral load had

gradually increased to 19.1 kN. From this point it was decided to increase the displacement to observe the effect of higher curvatures on the performance of the concrete stress block. Fig 6.3 shows the increase in bar strain up to the point at which the logger unit range was lost at 4.8% strain, and indicates a sharp increase of strain in bar f13 (130mm from extreme compression fibre) at about 90mm displacement. The peak lateral load achieved was 21.2 kN at 93mm displacement. At 100mm displacement, the strain in bar f13 had reached 1.1% at a lateral load of 21.1 kN. Upon reverse loading to zero displacement, Fig 6.2 shows a softening of the force-displacement relationship, and a residual force at zero displacement of 13 kN. At this point, the test specimen itself had dilated by 4.75mm.

6.6 Analysis of Results from Initial Loading

The lack of restraint from insitu concrete binding to the void indentations is probably due to the effect of shrinkage and service load cracking. Support line shrinkage cracks had appeared at the fixed end 15 days after the topping was cast, and averaged about 0.1mm opening. Shrinkage cracking combined with the imposed midspan load, which was specifically placed to cause cracking, were obviously sufficient to fracture the section. In addition, the comparatively low topping concrete strength would have helped to reduce concrete tensile capacity.

The effect of increased curvature on compression block behaviour showed that some resilience exists in the outer web and soffit region of well constructed Hollow Core units. The peak displacement imposed was 100mm, equalling a lateral sway of 1.35%.

If we approximate the average steel stress at this stage as 1.2 times the nominal yield value of 430 MPa, the total force in the compression stress block is:

$$\begin{aligned} C_c &= 1.2 \cdot A_s \cdot f_y \\ &= 1.2 \cdot 4 \cdot 113 \cdot 430 = 233 \text{ kN} \end{aligned} \quad (6.1)$$

Assuming that the average strength of concrete is 45 MPa (including the infilled section of voids), then the depth of the neutral axis at capacity is:

$$\begin{aligned} c &= \frac{C_c}{0.85 f'_c \beta_1 b} \\ &= \frac{233 \text{ kN}}{0.85 \cdot 45 \cdot 0.73 \cdot 265} = 31 \text{ mm} \end{aligned} \quad (6.2)$$

Assuming a linear strain distribution:

$$\begin{aligned}\varepsilon_{s_{f13}} &= \frac{\varepsilon_c (d-c)}{c} & (6.3) \\ &= \frac{0.003 \cdot (130-31)}{31} = 0.0096 \approx 0.011 \text{ measured}\end{aligned}$$

This indicates that the concrete compression block was at least at the design ultimate strain of 0.003. The neutral axis depth of 30mm agrees with measurements taken at this stage of the test which indicated crack closing to about 35mm from the extreme compression fibre. Due to confinement effects as mentioned, the ultimate strain capacity will increase to values above 0.003 [10], although it is not straight forward in predicting a figure because we are dealing with semi-confined, slightly high-strength concrete. Using a curvature of 0.0096/31mm, the corresponding bar stresses, taken from the exact stress-strain measurements is:

$$\begin{aligned}\varepsilon_{f1} &= 9.7\% \approx 582 \text{ MPa} \\ \varepsilon_{f5} &= 6.8\% \approx 564 \text{ MPa} \\ \varepsilon_{f9} &= 3.9\% \approx 520 \text{ MPa} \\ \varepsilon_{f13} &= 1.0\% \approx 446 \text{ MPa}\end{aligned}$$

The total force derived from actual stress values is:

$$\begin{aligned}C_c &= A_b \sum_i f_{si} & (6.4) \\ &= 113 \cdot (582 + 564 + 520 + 446) = 239 \text{ kN}\end{aligned}$$

The corresponding moment about the neutral axis is:

$$M = A_b \sum_i f_{si} (d_i - c) + C_c c \left(1 - \frac{\beta_1}{2}\right) \quad (6.5)$$

$$\begin{aligned}M &= 113 \cdot [(582 \cdot 1000) + (564 \cdot 700) + (520 \cdot 400) + (446 \cdot 100)] + (239,000 \cdot 20) \\ &= 144 \text{ kNm}\end{aligned}$$

The required point load at the sway end: $P = \frac{144 \text{ kNm}}{7.4 \text{ m}} = 19.5 \text{ kN}$ corresponds to the measured lateral load of 21.1 kN. If a curvature of 0.011/31mm had been used, the calculated moment would have been in closer agreement.

Force-Displacement from initial loading

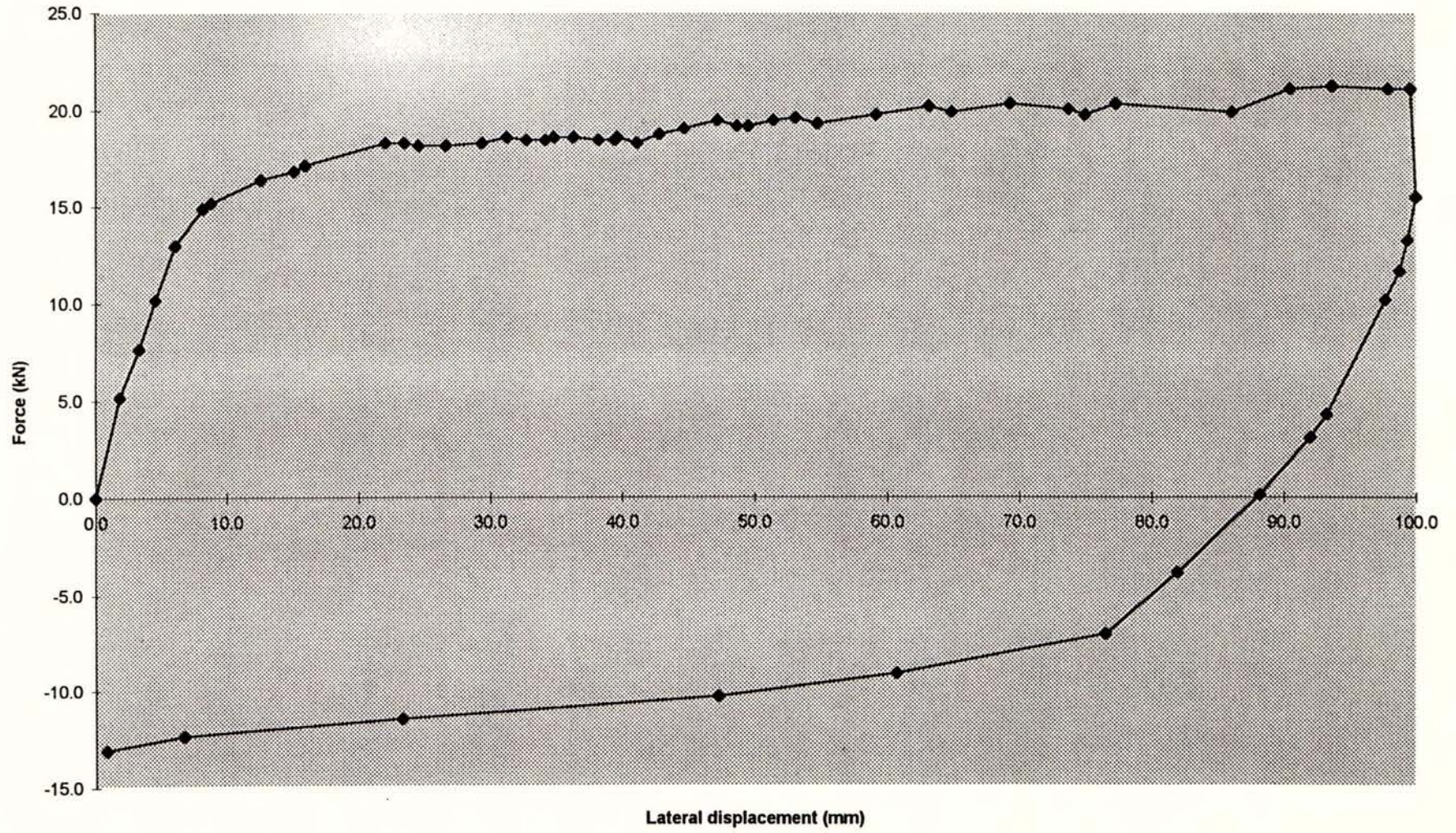


Fig 6.2: Load-displacement curve of initial loading stage

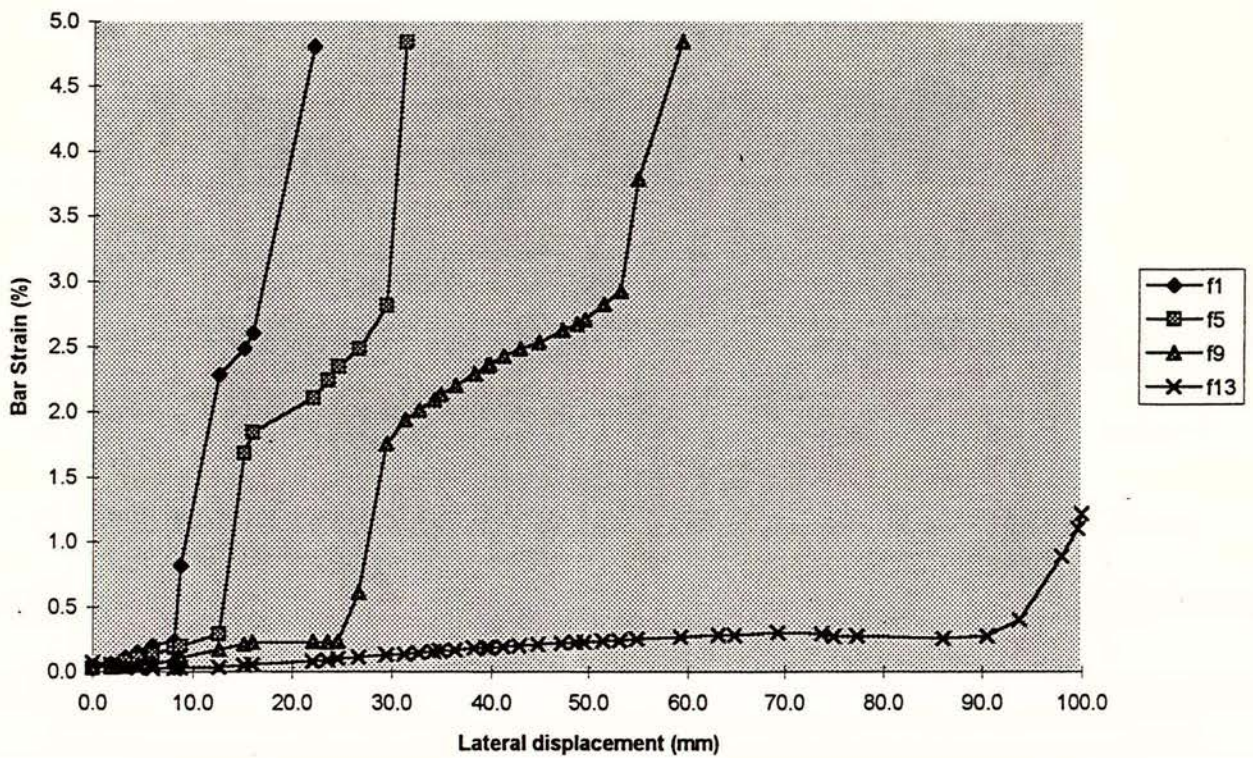


Fig. 6.3: Bar strain development under increasing lateral displacement

The bar strains used in this analysis include some small additional strain developed through negative bending moment at the support. The maximum bar stress developed under the applied cracking load was 288 MPa. At the start of the test the average bar stress under unit self weight plus superimposed dead load was 75 MPa.

Figs. 6.4 show curvature plotted against lateral displacement up to the point that the strain gauges failed. These measurements were arrived at by taking the difference in strain between adjacent bars along the critical crack and dividing by the bar spacing:

$$\psi = \frac{\Delta \epsilon}{\Delta c} = \frac{\Delta \epsilon_s}{s} \quad (6.6)$$

Fig. 6.4 b: shows a linear increase in the average curvature over the displacement range plotted. From these graphs, a moment curvature relationship may be constructed, where the moment is equal to the ram force P acting over a lever arm of 7.4m. The corresponding curvature is the average along the section, as plotted in Fig 6.4 b. The moment-curvature diagram is plotted up to a curvature corresponding to a lateral sway 55mm, which is approximately equal to a displacement ductility factor $\Delta u / \Delta y$ of 6.

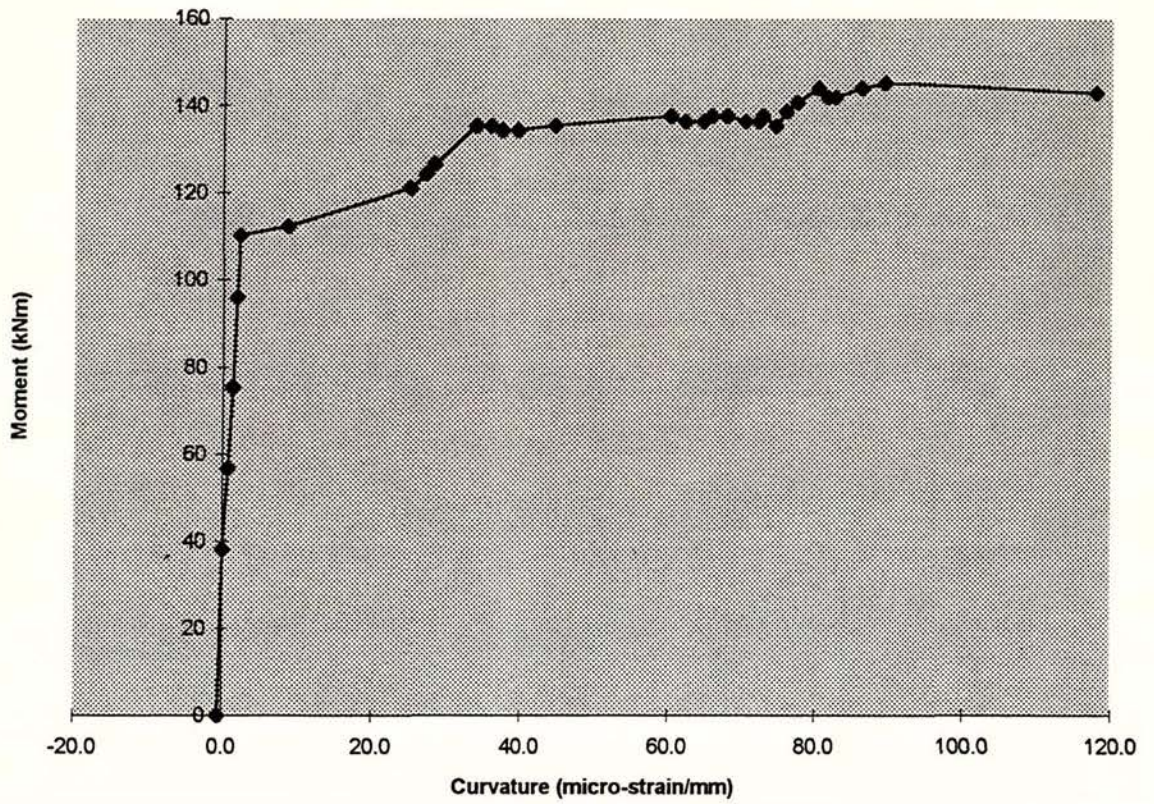


Fig 6.4 a: Moment-curvature relationship for initial loading stage, 0 - 55mm

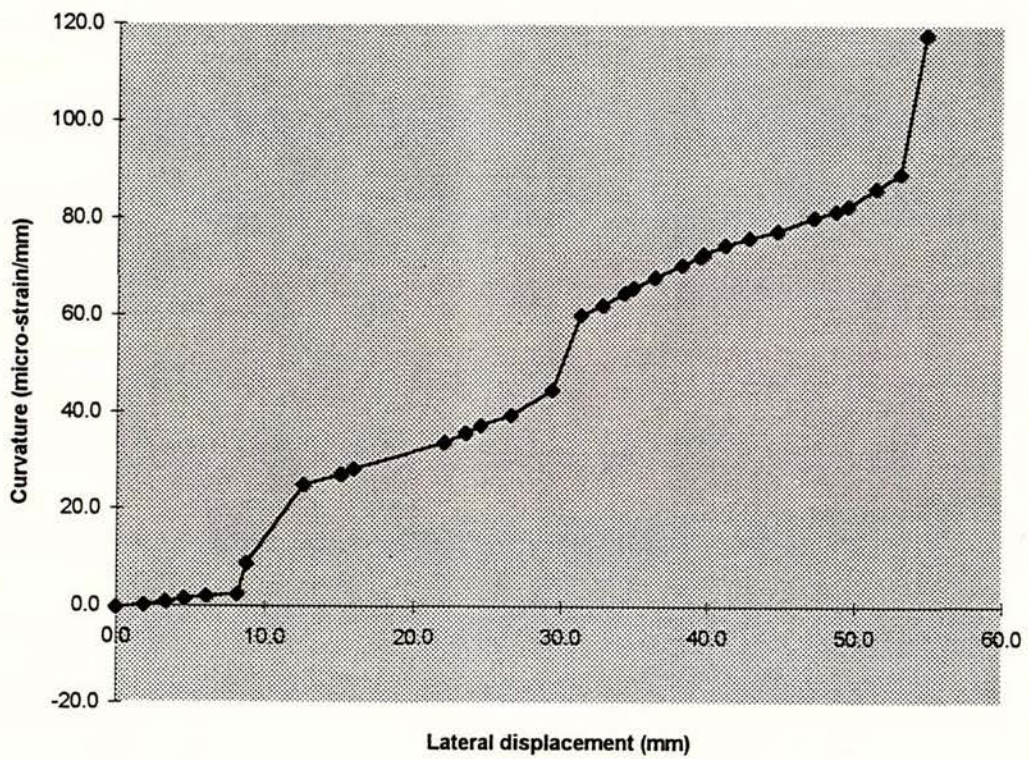


Fig 6.4 b: Average curvature plotted against lateral displacement

6.7 Results from Second Loading

The behaviour of stage two of this test is illustrated on Fig 6.6

In the second loading stage, an axial force of 400 kN was applied to simulate chord compression forces (section 6.4), and then the unit support was laterally displaced. Because of the existing load history, the small displacement stiffness of the support detail was less than for the initial loading. However, unlike the initial load stage, the unit did not exhibit elasto-plastic behaviour, but rather a gradually decreasing stiffness up the maximum lateral displacement. This resulted in a peak lateral force of approximately three times that of the initial loading stage. On reverse loading, the section stiffness had dropped considerably, although a similar peak load was obtained at the same displacement.

At this stage, localised upward buckling of the HD12 bars had caused the topping concrete to spall (Fig 6.5). The existing crack along the edge of the topping concrete and precast unit had become more pronounced, with a maximum crack opening of 0.3mm, and shear slippage had occurred along the critical crack, in the order of 1mm.

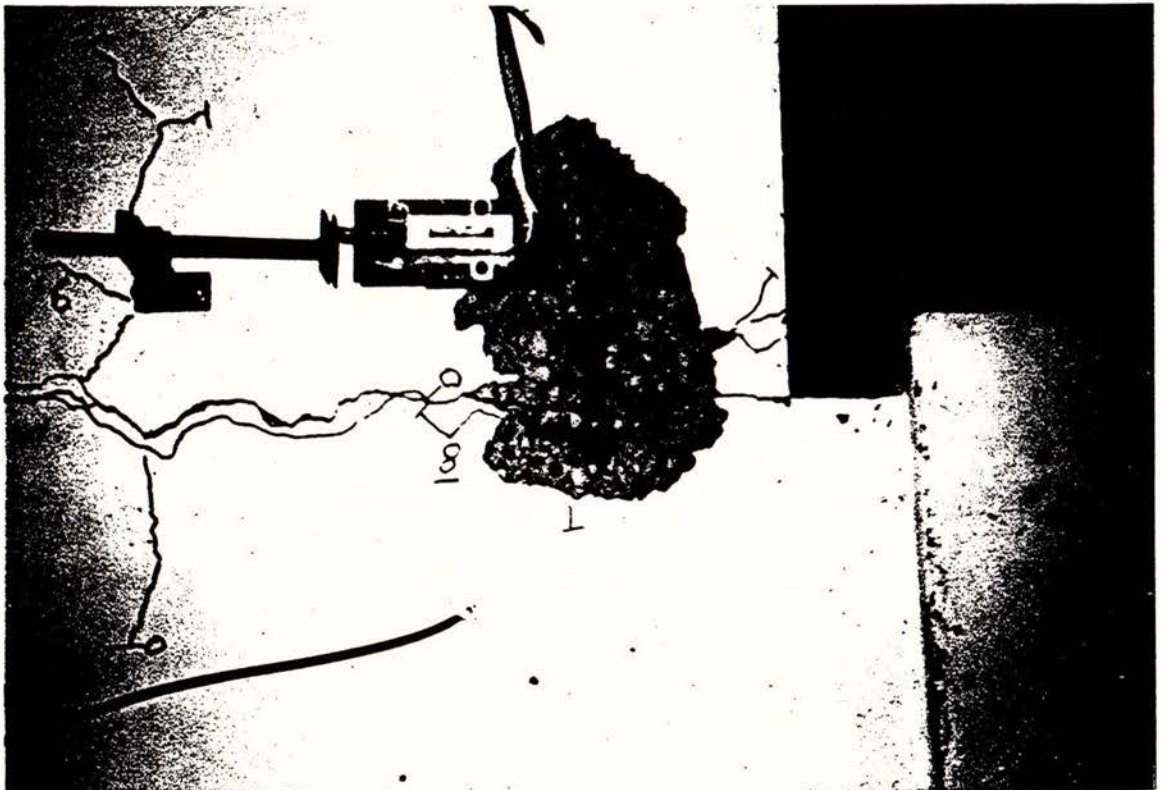


Fig 6.5: Buckling of top steel due to cyclic loading

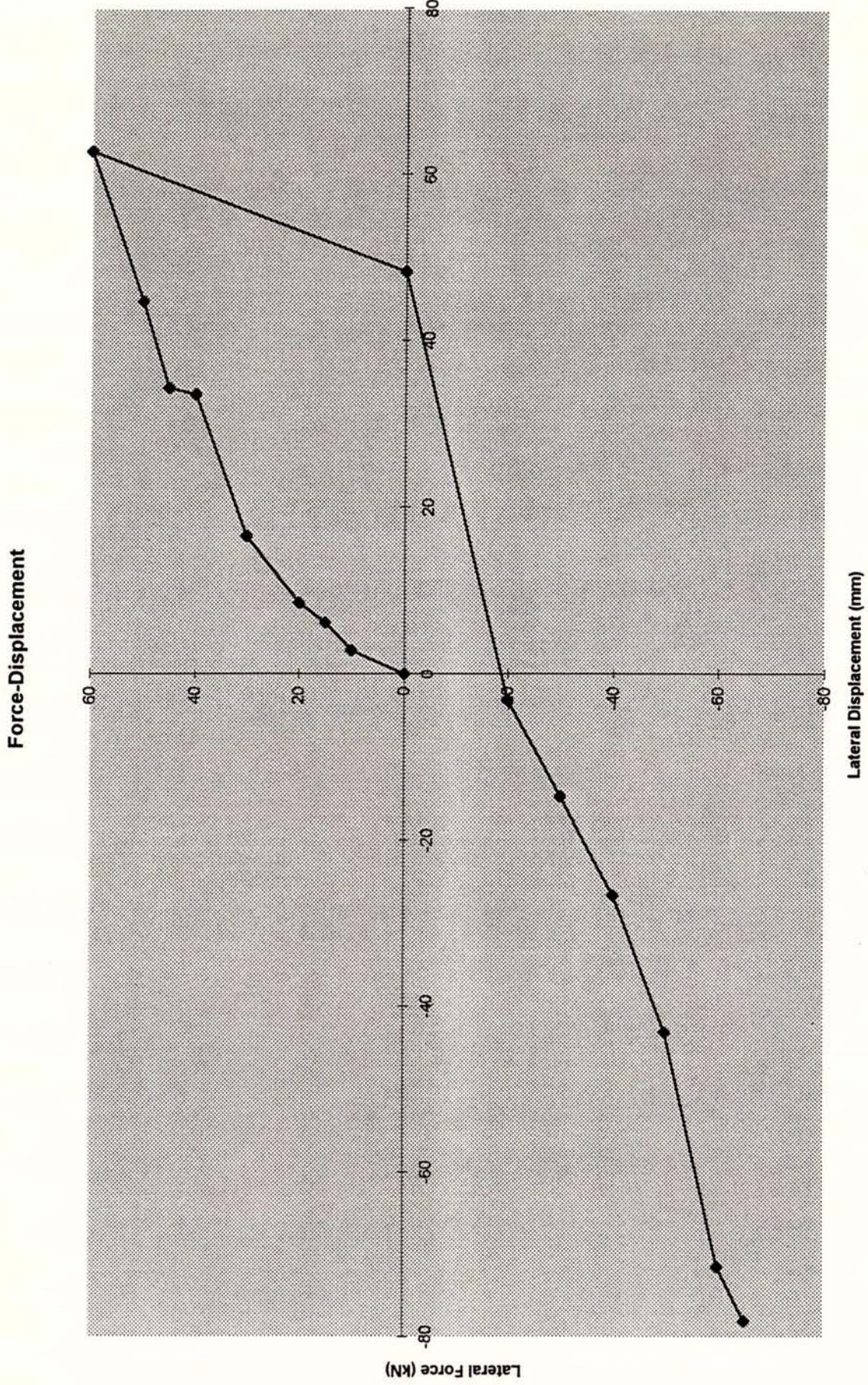


Fig 6.6: Load-displacement diagram for second load stage (400 kN compression)

6.8 Analysis of Results from Second Loading

At this stage of the test, readings from the strain gauges at the critical section had been lost and the bars were undergoing buckling due to the loading regime. Because of this it is not possible to estimate the axial force contribution of the reinforcing steel, although it would certainly be less than the peak reinforcing force under a monotonic loading.

The amplitude of bar buckling was approximately equal to the diameter of the bars, and the components of buckling showed a considerable uplift effect on the mesh wire that restrained the bars adjacent to the critical crack. The uplift components caused an increase in crack opening between the Hollow Core unit and the topping at the edges of the slab.

6.9 Conclusions of the Sway and Axial Load Test

The first load stage of this test examined the effects of insitu concrete binding to the ends of units and the ability of the outer webs of the Hollow Core unit to sustain large compressive strains.

Concrete binding was found not to be an issue, as the unit showed elasto-plastic behaviour characteristic of a ductile member at an early stage of the test. The effects of concrete binding were probably alleviated by a combination shrinkage cracking and cracking under service loads. The examination of binding to the void indentations was seen to be important, as this appeared to be a significant factor in the fracture of the unit in the first loss of support test (section 3).

The outer web and soffit region of the Hollow Core unit showed an ability to sustain compression strain in excess of the concrete code [1] ultimate value of 0.003. It is probable that the confinement effect produced by the unit being "clamped" between the insitu topping and the support is responsible for this increase in strain capacity. The lateral displacement applied to achieve this level of strain was higher than would normally be expected in a floor diaphragm. However, the comparison building that exhibited floor failure in the Los Angeles earthquake of January 1994 may have experienced excessive displacements due to a combination of a failed chord tie, and very flexible cantilevered columns. Photographs of the residual structure certainly indicate columns that have travelled a significant distance away from the vertical.

The second stage of loading concluded more about the effects of bar buckling than anything else, and the results may not be encouraging. This part of the test strongly indicated that for a floor that has been forced to dilate due to frame action and undergo a series of cycles,

the topping may begin to uplift through the buckling of continuity or starters bars. This effect would apply mainly to interior supports where significant quantities of negative steel have been incorporated for continuity, and the topping mesh also runs over the support. The greater the quantity of steel, the more pronounced is the net effect. Another consideration is that the spalling around the bars is significant, and for layers of bars at close spacings, much of the rigid shear capacity of the diaphragm could be lost through excessive spalling along the support line. In this test, a minimal number of bars were present, but the bar buckling effect was noticeable even for a cycle of dilation and contraction that did not exceed 15mm.

6.10 Recommendations from Sway and Axial Load Test

The performance of the unit in cantilever bending through the plane of the floor indicated that confinement is beneficial, as well as the presence of an approximately uniform concrete compression zone. This would suggest that in opposition to the support pull off tests in which tension effects are of primary concern, the presence of a depth of insitu concrete in the voids may be beneficial.

The observed bar buckling would lead to an instant recommendation that the diameter of bar used in toppings of normal thickness should not exceed 12mm diameter. Limiting the bar to this size will likewise limit the uplift component of buckling, which would be quite severe with a 16mm diameter bar.

6.11 Recommendations for Future Research

Suggested future research is that a further test should be conducted on a unit with sizeable quantities of top steel, in which a high level of axial compression is applied, and the unit swayed in cantilever action. This will test whether web crushing could be a problem, and if so, would set the upper limits to the problem. Concurrently, this test would examine the effects of bar buckling on spalling and delamination of the topping concrete. A separate study of the potential effects of bar buckling in topping slabs may be advisable.

References

- 1 "Code of Practice for the Design of Concrete Structures, NZS 3101:1982 and Amendment No. 1 :1989, Standards Association of New Zealand, Wellington.
- 2 N L Scott, "Performance of Precast Prestressed Hollow Core Slab with Composite Topping", Journal of Prestressed Concrete Institute, March/April 1973
- 3 "Guidelines for the Use of Structural Precast Concrete in Buildings", Centre for Advanced Engineering, University of Canterbury, New Zealand.
- 4 "Shear at the Interface of Precast and Insitu Concrete", FIP Guide to Good Practice, Federation Internationale de la Precontrainte, Wexham Springs 1982.
- 5 "Shear at the Interface of Precast and Insitu Concrete", FIP Technical Report, Federation Internationale de la Precontrainte, Wexham Springs 1978.
- 6 J C Mejia-McMaster and R Park, "Precast Concrete Hollow Core Floor Unit Support and Continuity", Research Report 94/4, Department of Civil Engineering, University of Canterbury, New Zealand.
- 7 "Precast Hollow Core Floors", FIP , Thomas Telford, London 1988.
- 8 G Hill, "Strain Gauging Technique as at January 1992", Civil Engineering Department, University of Canterbury, Canterbury, New Zealand 1992.
- 9 A S G Bruggeling and G F Huyghe, "Prefabrication with Concrete", A A Balkema, Rotterdam 1991.
- 10 R Park and T Paulay, "Reinforced Concrete Structures", John Wiley and Sons Inc 1975.
- 11 T Y Lin and Ned H Burns, "Design of Prestressed Concrete Structures", John Wiley and Sons Inc 1982.
- 12 "Code of Practice for the General Structural Design and Design Loadings for Buildings, NZS 4203:1992, Standards Association of New Zealand, Wellington.